AD-A069 439 GULF AND WESTERN APPLIED SCIENCE LABS WALTHAM MA F/G 6/4
SENSORY MECHANISM MODELING.(U)
FEB 79 J BORAH, L R YOUNG, R E CURRY F33615-76-C-0039
UNCLASSIFIED AFHRL-TR-78-83 NL

| OF |
AD A069 439

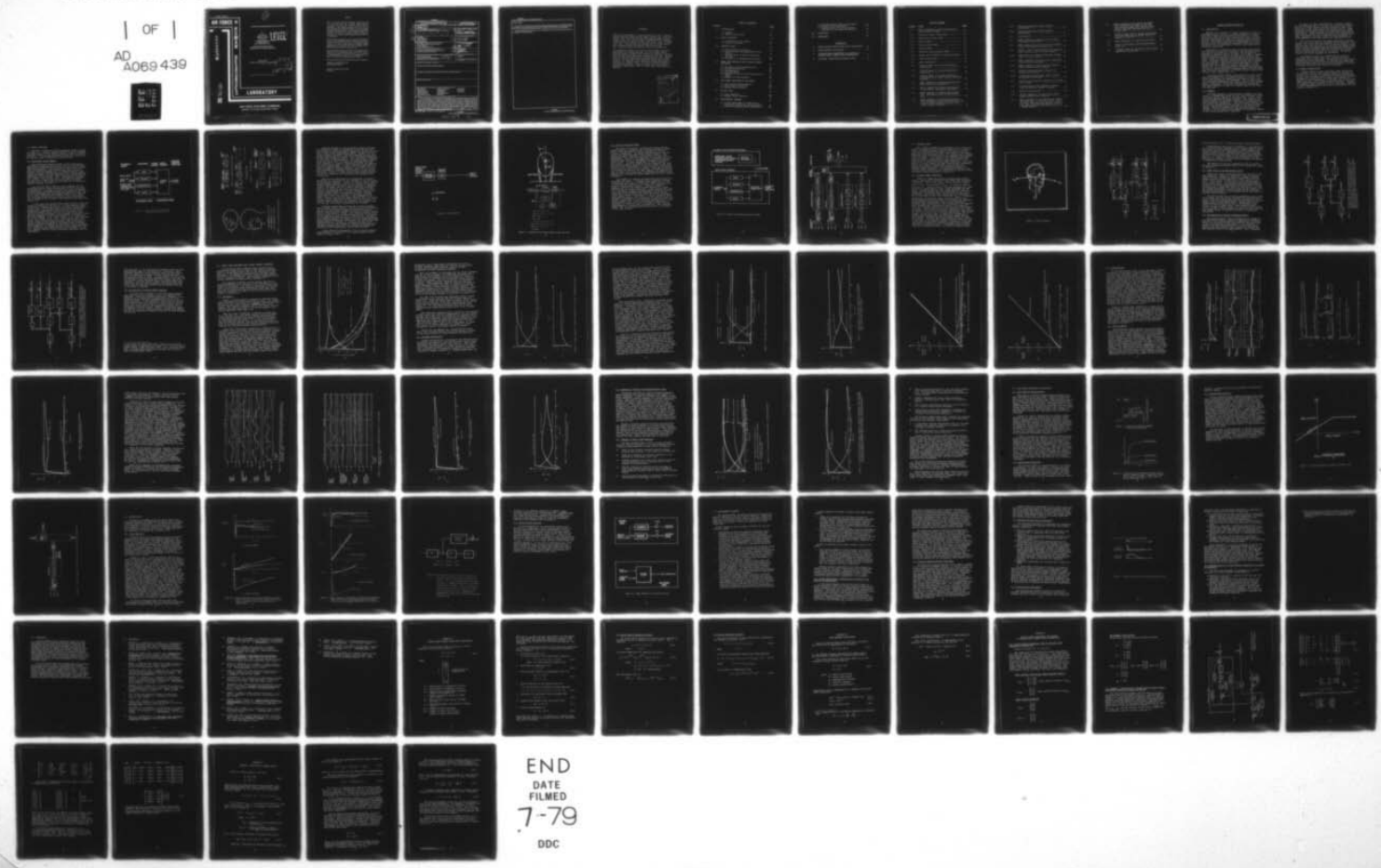

END
DATE FILMED
7-79
DDC

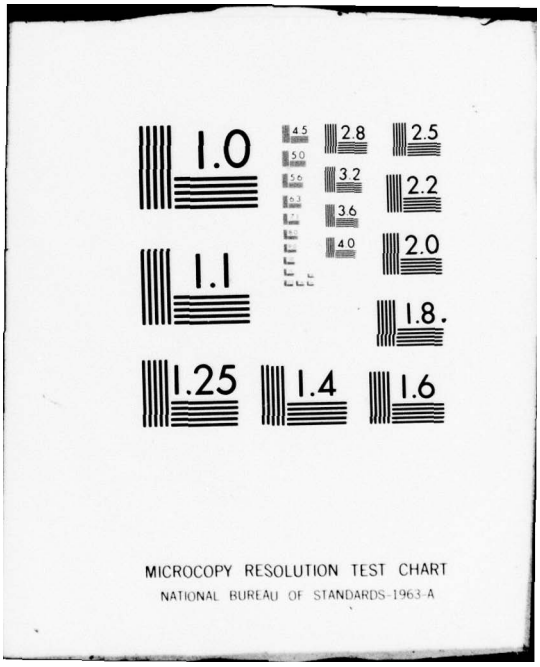
1.0
1.1
1.25
1.4
1.6
1.8
2.0
2.2
2.5
2.8
3.2
3.6
4.0
4.5
5.0
5.6
6.2
MICROCOPY RESOLUTION TEST CHART
NATIONAL BUREAU OF STANDARDS-1963-A

AFHRL-TR-78-83

AIR FORCE

HUMAN RESOURCES

LABORATORY

SENSORY MECHANISM MODELING (Final Report)

By

Joshua Borah
Laurence R. Young
Renwick E. Curry
Gulf + Western
Applied Science Laboratories
335 Bear Hill Road
Waltham, Massachusetts 02154

LEVEL II

ADVANCED SYSTEMS DIVISION
Wright-Patterson Air Force Base, Ohio 45433

February 1979
Final Report for Period June 1977 – September 1978

AIR FORCE SYSTEMS COMMAND
BROOKS AIR FORCE BASE, TEXAS 78235

NOTICE

When U.S. Government drawings, specifications, or other data are used for any purpose other than a definitely related Government procurement operation, the Government thereby incurs no responsibility nor any obligation whatsoever, and the fact that the Government may have formulated, furnished, or in any way supplied the said drawings, specifications, or other data is not to be regarded by implication or otherwise, as in any manner licensing the holder or any other person or corporation, or conveying any rights or permission to manufacture, use, or sell any patented invention that may in any way be related thereto.

This final report was prepared by Gulf + Western, Applied Science Laboratories, 335 Bear Hill Road, Waltham, Massachusetts 02154 under contract F33615-76-C-0039, project 6114, with Advanced Systems Division, Air Force Human Resources Laboratory (AFSC), Wright-Patterson Air Force Base, Ohio 45433. Mr. William B. Albery (ASM) was the Contract Monitor for the Laboratory.

This report has been reviewed and cleared for open publication and/or public release by the appropriate Office of Information (OI) in accordance with AFR 190-17 and DoDD 5230.9. There is no objection to unlimited distribution of this report to the public at large, or by DDC to the National Technical Information Service (NTIS).

This technical report has been reviewed and is approved for publication.

GORDON A. ECKSTRAND, Director
Advanced Systems Division

RONALD W. TERRY, Colonel, USAF
Commander

Unclassified

SECURITY CLASSIFICATION OF THIS PAGE (When Data Entered)

REPORT DOCUMENTATION PAGE

READ INSTRUCTIONS BEFORE COMPLETING FORM

1. REPORT NUMBER: AFHRL-TR-78-83	2. GOVT ACCESSION NO.
3. RECIPIENT'S CATALOG NUMBER	
4. TITLE (and Subtitle): SENSORY MECHANISM MODELING (Final Report)	5. TYPE OF REPORT & PERIOD COVERED: Final rept. June 1977 – September 1978
6. PERFORMING ORG. REPORT NUMBER	
7. AUTHOR(s): Joshua Borah, Laurence R. Young, Renwick E. Curry	8. CONTRACT OR GRANT NUMBER(s): F33615-76-C-0039
9. PERFORMING ORGANIZATION NAME AND ADDRESS: Gulf + Western Applied Science Laboratories, 335 Bear Hill Road, Waltham, Massachusetts 02154	10. PROGRAM ELEMENT, PROJECT, TASK AREA & WORK UNIT NUMBERS: 62205F, 6114/901, 17 19
11. CONTROLLING OFFICE NAME AND ADDRESS: HQ Air Force Human Resources Laboratory (AFSC), Brooks Air Force Base, Texas 78235	12. REPORT DATE: February 1979
	13. NUMBER OF PAGES: 88
14. MONITORING AGENCY NAME & ADDRESS (if different from Controlling Office): Advanced Systems Division, Air Force Human Resources Laboratory, Wright-Patterson Air Force Base, Ohio 45433	15. SECURITY CLASS. (of this report): Unclassified
	15a. DECLASSIFICATION/DOWNGRADING SCHEDULE

16. DISTRIBUTION STATEMENT (of this Report)

Approved for public release; distribution unlimited.

17. DISTRIBUTION STATEMENT (of the abstract entered in Block 20, if different from Report)

18. SUPPLEMENTARY NOTES

19. KEY WORDS (Continue on reverse side if necessary and identify by block number)

flight simulation	neural sensory receptors	motion effects
motion perception	vestibular sensors	linearvection
orientation perception	tactile sensors	circularvection
optimal estimation	proprioceptive sensors	
sensory system modeling	visual effects	

20. ABSTRACT (Continue on reverse side if necessary and identify by block number)

Pilots use information from a variety of sensory mechanisms to determine their estimate of orientation and motion. An understanding of this process and a quantitative model are essential for development of effective simulator motion cueing devices. A multisensory model for dynamic spatial orientation is being developed for this purpose. Aircraft or simulator motion is translated into stimuli which are processed by dynamic models of the appropriate sensors (visual, vestibular, tactile, and proprioceptive), and are then fed to a central estimator which has been modeled as a linear optimal estimator, specifically a steady state Kalman Filter. In addition to the linear estimation process, some non-linear effects, such as the well documented delay in onset of visually induced motion, require non-linear additions to the model. Such additions have been kept to a minimum so as to retain the uniqueness and conceptual appeal of a linear optimization algorithm.

(Over)

DD FORM 1 JAN 73 1473 EDITION OF 1 NOV 65 IS OBSOLETE

Unclassified

SECURITY CLASSIFICATION OF THIS PAGE (When Data Entered)

410 539 LB

Item 20 Continued:

The model has been implemented as a computer program and has predicted some of the important qualitative characteristics of human dynamic spatial orientation under combined wide field visual motion and platform motion. Several types of special tactile and proprioceptive cues are also being considered but have not been validated.

The modeling effort has underscored the need for additional data in some areas and several experiments have been suggested to help fill these gaps.

FOREWARD

This report documents a study conducted by Gulf + Western Applied Science Laboratories under Contract No. F33605-76-C-0039, and covers the period from January 1976 through August 1978. An interim report (AFHRL-TR-77-70) provides a more detailed account of the first year's work, through July 1977. The project was managed by Dr. David Sheena, with Joshua Borah as principal investigator and Drs. Laurence Young and Renwick Curry as consultants.

The sponsoring agency was the Air Force Human Resources Laboratory at Wright-Patterson Air Force Base, where William Albery and Max Fiore served as technical contract monitors and the program was overseen by Don Gum. Several other people have assisted in reviewing the work, among them Dr. Charles Oman (Massachusetts Institute of Technology), Dr. Raphael Sivan (Technion Israel Institute of Technology), Andrew Junker (Air Force Aerospace Medical Research Laboratory), Patricia Knoop (Air Force Human Resources Laboratory), and Dr. David Quam (University of Dayton).

TABLE OF CONTENTS

SECTION		PAGE
1.0	INTRODUCTION	9
	1.1 Summary	9
	1.2 Report Organization	10
2.0	MODEL STRUCTURE	11
	2.1 Individual Sensor Models	11
	2.2 Central Processor	17
3.0	INTERNAL MODEL	20
	3.1 Internal Model Structure	20
	3.2 Input Spectra and Measurement Noise Ratios	23
	3.3 Consideration of Sensor Threshold Effects	23
	3.4 Decoupling of Independent Channels	26
4.0	MODEL TIME RESPONSES WITH LINEAR CENTRAL PROCESSOR	27
	4.1 Yaw Motion and Circularvection	27
	4.2 Forward Acceleration	29
	4.3 Linearvection	36
	4.4 Tilting Motion	36
	4.5 Response to Tactile and Proprioceptive Input	45
	4.6 Summary of Time Respones	45
5.0	NON-LINEAR ADDITIONS TO THE MODEL	49
	5.1 Cue Conflict Non-Linearity	49
	5.2 Large Angle Correction	49
	5.3 Saccule Non-Linearity	51
6.0	ACTIVE PILOT	54
	6.1 Input Spectrum	54
	6.2 Control Stick Position	58
7.0	EXPERIMENTAL PROGRAM	60
	7.1 Flight Experiment to Study Motion Perception and Motion Cue Environment	61
	7.2 Vibration Masking Effect Experiment	62

7.3 Minimum Platform Motion Experiment 63
7.4 G-Cueing Seat Experiment 63
7.5 Characteristics of Vibro-tactile Sensation on the Back and Buttocks 65

8.0 CONCLUSION 67

9.0 REFERENCES 68

APPENDICES

A STEADY-STATE KALMAN FILTER GAIN CALCULATION 71

B TIME RESPONSE CALCULATION 75

C INTERNAL MODEL PARAMETERS AND EXAMPLE OF STEADY-STATE KALMAN FILTER CONSTRUCTION 77

D DISCRETE, TIME-VARYING KALMAN FILTER 83

LIST OF FIGURES

FIGURE	TITLE	PAGE
2.1	Basic structure of motion and orientation perception model	12
2.2	Cyclopian sensor coordinates	13
2.3	Semicircular canal model	13
2.4	Otolith model	13
2.5	Visual sensor model	13
2.6	Tactile model	15
2.7	Head-neck proprioception model	16
2.8	Motion and orientation perception model .	18
2.9	Time history model	19
3.1	Head coordinates	21
3.2	Internal model for visual-vestibular interaction	22
3.3	Internal model for tactile-vestibular interaction	24
3.4	Internal model for visual-vestibular interaction with visual horizon reference included	25
4.1	Model response to combined platform and wide visual field yaw motion	28
4.2	Model response to forward acceleration "in the dark" (vestibular cues alone) ...	30
4.3	Model response to forward acceleration with confirming visual field velocity cues	32
4.4	Model response to forward acceleration with confirming visual field velocity cues, 5 m/sec visual saturation limit, and a visual horizon reference	33

4.5a	Velocity perception during forward acceleration	34
4.5b	Velocity perception during forward acceleration	35
4.6	Linearvection	37
4.7	Model response to pitch-up "in the dark" (vestibular cues alone)	38
4.8	Model response to pitch-up with confirming visual field angular velocity cue	39
4.9	Typical results from subjective orientation angle tracking task in a link trainer	41
4.10	Subjective roll velocity magnitude estimation in a link trainer	42
4.11	Model response to pitch-up with confirming visual horizon reference	43
4.12	Model response to pitch-up with vehicle-fixed visual horizon reference	44
4.13	Tactile-vestibular model response to forward acceleration	46
4.14	Proprioceptive-vestibular model response to lateral acceleration	47
5.1	Conflict non-linearity combined with Kalman filter model	50
5.2	Circularvection step response of model with cue conflict element included	50
5.3	Saccule non-linearity	52
5.4	Otolith component of time history model showing saccule non-linearity	53
6.1	Model response to yaw acceleration impulse (velocity step) in the dark, using internal model with wide band angular acceleration input spectrum approximating that of a random impulse	55

6.2 Model response to yaw angular acceleration step (velocity ramp) in the dark, using internal model with angular acceleration spectrum approximating that of a step (1/s) 56

6.3 Internal model used to derive both steady-state and time-varying Kalman filters in figures 6.1 and 6.2 57

6.4 Model extension to include active pilot . 59

7.1 Visual field motion with platform motion onset cue 64

C.1 Internal model for yaw motion with visual-vestibular interaction 79

SENSORY MECHANISM MODELING

1.0 INTRODUCTION

Whether in an aircraft or flight simulator, pilots use information from a variety of sensory mechanisms to determine their estimate of orientation and motion. An understanding of this process and a quantitative model are essential for development of effective simulator motion cueing devices. This report describes the development of a multi-sensory motion and orientation perception model which will be used to aid in development of current and future motion simulation techniques.

The model is a potential tool for objectively gauging the fidelity of simulation strategies and the relative importance of different cueing devices. For example, on a maneuver by maneuver basis, the model can be used to compare perceived motions and forces created by an aircraft with those created by simulator cueing hardware and drive algorithms. Potential simulator deficiencies may thus be spotted prior to extensive subjective testing and sources of existing deficiencies, causing poor pilot performance or complaints that the simulation "doesn't feel right," may be identified. It is anticipated that the model will eventually help to address questions concerning the optimum and most cost effective combinations of platform motion, visual scene motion, g-seat stimulation, etc.

A previous report (Borah, Young and Curry, 1977) developed the framework for the modeling effort, including detailed descriptions of individual vestibular, visual, tactile, and proprioceptive system models. This is now reviewed and further development and exercise of the multi-sensory model is described. A specific experimental program has also been suggested to help fill several gaps in the existing data base.

1.1 Summary

The model employs a linear optimal estimator, in particular, a steady-state Kalman filter, to blend signals from individual dynamic models of the vestibular, visual, tactile and proprioceptive sensor systems. The resulting time domain estimate is the model's prediction of human motion and orientation "perception." Some non-linear effects, such as the well documented delay in onset of visually induced motion, require non-linear additions to the "central processor." We have attempted to keep such additions to a minimum so as to retain the uniqueness and conceptual appeal of the linear optimization algorithm.

The model has been implemented as a computer program and has predicted some of the important qualitative characteristics of human dynamic spatial orientation under combined wide field visual motion and platform motion. These responses are described along with suggestions for further improvements. Model response to tactile and proprioceptive cues has been tested in a preliminary way and appears to be quite reasonable, although a more thorough validation of these components must await additional experimental data.

The initial version of the model represents a passive subject with little advance knowledge of the stimulus. Two parallel approaches are described for model extension to the active pilot. One approach is to optimize the Kalman filter about the specific motion spectrum anticipated by the pilot, while a second technique calls for inclusion of aircraft control position as an input to the filter. Preliminary tests of the former approach are presented.

The modeling effort has underscored the need for additional data in some areas and a program has been suggested to fill these gaps. Several specific experiments are described which would help to validate and extend the model and which might also be directly applicable to design of motion cueing devices and drive algorithms.

1.2 Report Organization

Dynamic models of each individual sensor system and the structure of the multi-sensory model are reviewed in section 2.0. Section 3.0 contains a detailed description of the "internal model" used to derive the linear estimator, followed by a presentation of model time responses in section 4.0 and a discussion, in section 5.0, of non-linear model additions used to improve these responses. Section 6.0 explores model extension to the active pilot. Additional data requirements and some specific experiments are discussed in section 7.0.

2.0 MODEL STRUCTURE

The basic concept of the multi-sensory model is shown by Figure 2.1. Various sensors respond to the environment and send signals to the central nervous system or "central processor." The central processor blends this information to form an overall estimate of inertial state.

2.1 Individual Sensor Models

The vestibular sensors located in the non-auditory labyrinthine structure within each inner ear are the most thoroughly studied and well defined of the sensory systems under consideration. The semicircular canals are the rotation sensing component of the vestibular system and respond to angular acceleration as would a heavily damped torsion pendulum with some additional rate sensitivity and adaptation (Young and Oman, 1969; Goldberg and Fernandez, 1971; Ormsby, 1974; Young, 1974). For modeling purposes, the two sets of canals have been replaced by a single cyclopian set at the center of the head and are modeled as shown in Figures 2.2 and 2.3.

The otoliths which form the other component of the vestibular system, sense gravito-inertial force much like accelerometers. As shown in Figure 2.4, they are modeled as mechanical accelerometers with some additional rate sensitivity presumably due to afferent processing (Young and Meiry, 1968; Fernandez and Goldberg, 1976). Once again, the cyclopian system has been used for modeling purposes and is assumed to be located at the center of the head (see Figure 2.2).

It has long been observed that moving visual fields can induce a sensation of motion such as that sometimes experienced when a neighboring train in a railway station begins to pull away. It has been shown that visual self-motion sensation is proportional to the velocity of the background peripheral vision field up to a saturation level and that the effectiveness of the stimulus is related to the spatial frequency, contrast and resolution of elements in the field (Brandt, et al. 1973; Brandt, et al. 1975; Berthoz et al. 1975; Held, et al. 1974). The current model considers only out-the-window peripheral view fields such as moving clouds or star patterns and specifically excludes cockpit instrument readings or structures such as recognizable landmarks. In several specific cases, discussed later on, a visual horizon reference has been included. In general, however, static visual orientation references are not considered.

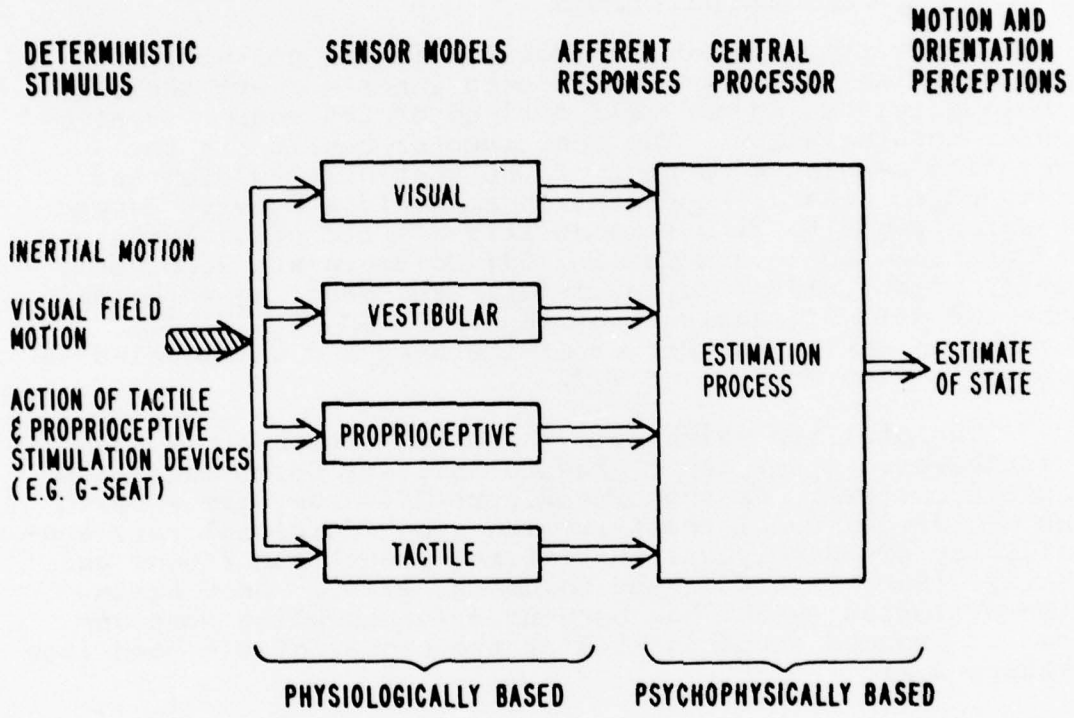

Figure 2.1 Basic structure of motion and orientation perception model

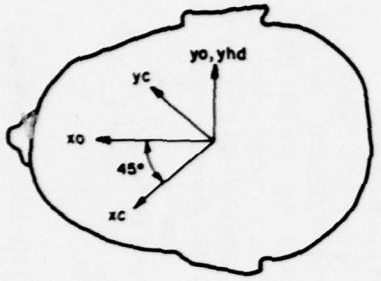

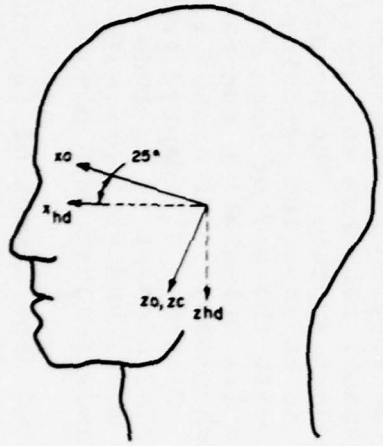

HEAD COORDINATES ≡ (xhd , yhd , zhd)

CANAL COORDINATES ≡ (xc , yc , zc)

OTOLITH COORDINATES ≡ (xo , yo , zo)

Figure 2.2 Cyclopian Sensor Coordinates

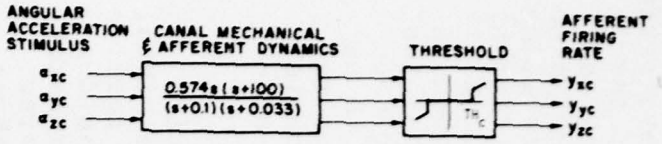

Figure 2.3 Semicircular Canal Model

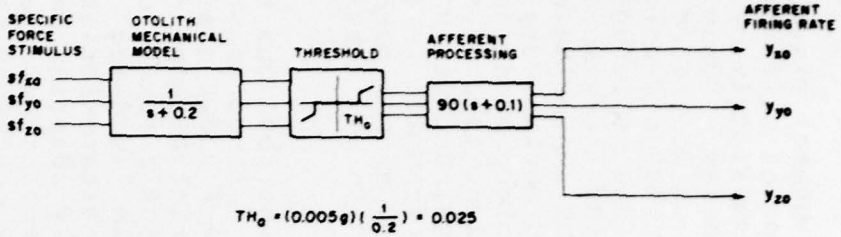

Figure 2.4 Otolith Model

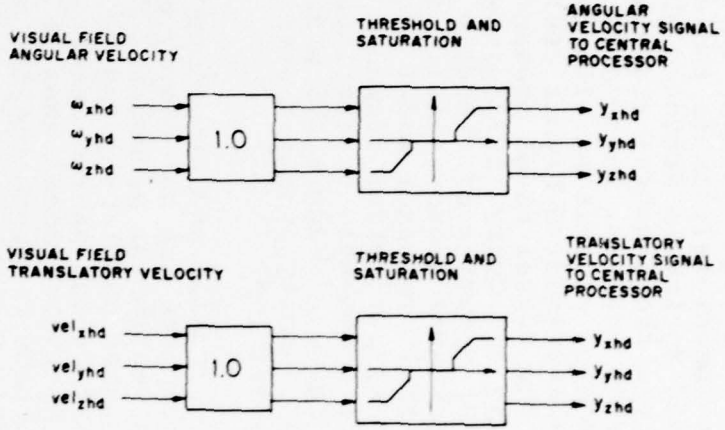

Figure 2.5 Visual Sensor Model

Although movement in the peripheral visual field may not immediately cause the sensation of self-motion, the field motion is detected almost immediately by the eye after only a short neural transmission delay. Dynamics of the visual sensors, therefore, have been modeled as unity and dynamics associated with onset of the self-motion sensation are ascribed to higher centers. This represents a revision of the visual model presented in the interim report (Borah, Young and Curry, 1977) in which the approximately first order dynamics of visually induced motion were included in the visual sensor model. It has since been found that the central processor model is sufficient to produce the necessary perceptual response dynamics, and it is felt to be more reasonable to attribute such dynamics to the central processor. Figure 2.5 shows visual sensor models consisting of unity dynamics with saturation and threshold nonlinearities.

Tactile and proprioceptive contributions to motion perception are not nearly as well defined as are the visual and vestibular elements. Figure 2.6 shows a simple tactile receptor model proposed as an initial attempt to consider "seat-of-the-pants" sensation during aircraft or simulator flight. The model uses as a single "lead-lag" transfer function to represent the major characteristics of three distinct mechanoreceptors: rapidly adapting Pacinian corpuscles usually found in subcutaneous tissue, and more slowly adapting type I and type II cutaneous receptors (Lowenstein, 1971; Iggo and Muir, 1969; Chambers et al, 1972). Several such tactile model elements will be used to consider forces applied to various areas of the body. The current model version uses two elements, one representing the seat pan and another representing the backrest.

Although proprioceptive sensation involves numerous muscle length, muscle tension, and joint position receptors, the initial multi-sensory model considers only muscle spindle (length sensor) response to lateral gravito-inertial force on the head-neck system. The head-neck system, which may be thought of as an inverted pendulum that is balanced on the body trunk with the aid of neck muscles, provides a very important spatial orientation cue and, among applicable proprioceptive mechanisms, lends itself to the most straight forward modeling. Figure 2.7, adapted from Gum (1973), represents an initial attempt to include proprioception in the multi-sensory model and will probably be refined and expanded as more experimental data become available.

A more detailed development of the individual sensory system models can be found in the interim report (Borah, Young and Curry, 1977).

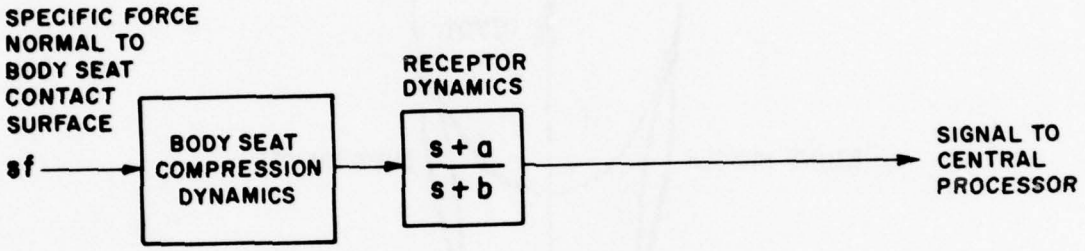

$$\tau_b = \frac{1}{b} \approx 10\text{msec}$$

$$\frac{a}{b} = \frac{1}{10}$$

Figure 2.6 Tactile Model

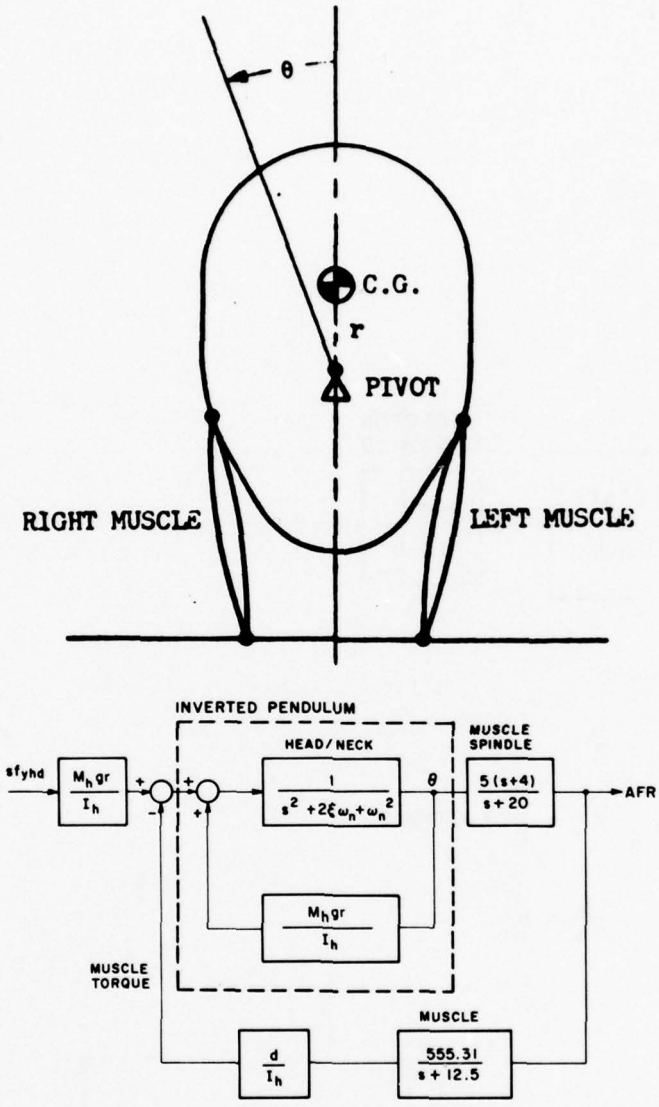

$d \equiv$ muscle lever arm = .075 m

$I_h \equiv$ head moment of inertia = .0304 kg

$M_h \equiv$ head mass = 4.6 kg

$\omega_h \equiv 7.81 \frac{rad}{sec}$

$r \equiv$ inverted pendulum length = .0498 m

$sf_{zhd} \equiv$ specific force parallel to body axis

$sf_{yhd} \equiv$ lateral specific force

$\xi \equiv 0.64$

Figure 2.7 Head-Neck Proprioception Model (after Gum, 1973)

2.2 Central Processor Model

The central processor, representing central nervous system function, is modeled as an optimal estimator which weights each information channel according to certain a priori assumptions. To assign optimal weights, the processor must have knowledge of the sensor dynamics, the expected stimulus spectrum, and the noise in each sensor measurement. This set of assumptions is referred to as the Internal Model since it represents the system's knowledge about itself. If these assumptions include linearity, stationarity, and white Gaussian noise processes, the optimal linear estimator reduces to the well known steady state Kalman filter, and weights or "Kalman gains" can be chosen to minimize rms error of the estimate. Although the biological system is certainly far more complex, our approach has been to start with relatively straightforward Kalman filter blending and increase the model complexity only as it proves necessary.

Two FORTRAN IV computer programs have been written to implement the model: a "Kalman filter parameter" program to calculate gains for a steady-state Kalman filter, and a "Time History" program to calculate time response of the model to deterministic stimuli. Figure 2.8 shows a schematic view of the computer model employing a linear filter alone as central processor. After optimal gains are set, time domain stimuli corresponding to aircraft or simulator motion are processed by individual sensor models (which may include non-linearities) and fed to the steady-state Kalman filter. The filter, in turn, estimates state variables corresponding to perception of inertial state and spatial orientation. A more detailed schematic of the time history model, with visual and vestibular components, is presented in Figure 2.9, and the method used for digital implementation is presented in Appendix B. The "internal model" used to calculate Kalman filter gains is described in the next section.

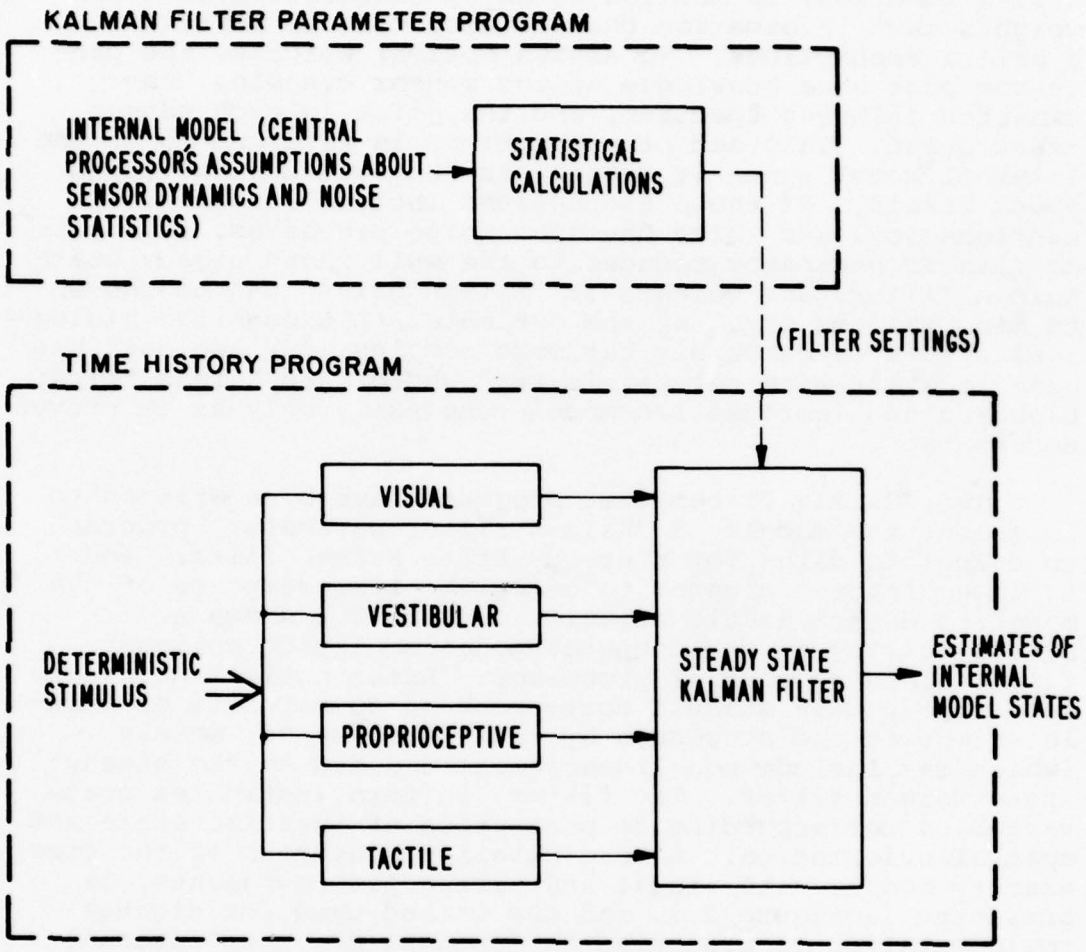

Figure 2.8 Motion and orientation perception model

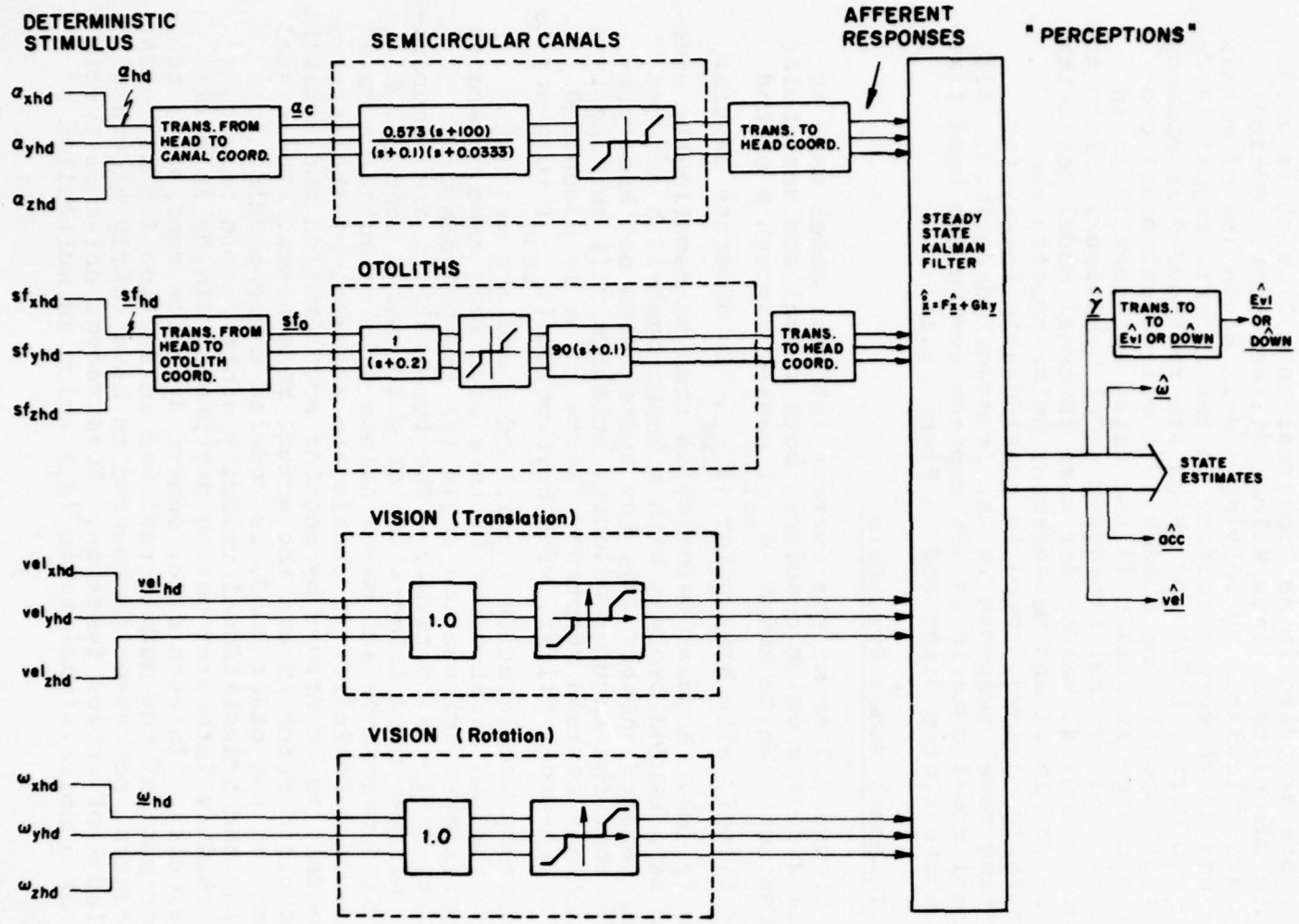

Figure 2.9 Time History Model

3.0 INTERNAL MODEL

The a priori assumptions attributed to the central processor are embodied in an "internal model" which is used only to calculate optimum Kalman filter gains. Optimal gains are calculated by solving a well known set of matrix equations which were specified in the interim report (Borah, Young and Curry, 1977) and which are reproduced in Appendix A of this report. Any change in the internal model produces a change in Kalman filter gains and results in an alteration of central processor model behaviour. Since the proper or logical values for some internal model parameters such as the input and measurement noise spectra are essentially unknown, there is considerable leeway for adjusting model response in the framework described. All internal model quantities are represented in the head fixed coordinate system diagramed in Figure 3.1.

3.1 Internal Model Structure

Figure 3.2 shows the current internal model used to create a filter which considers both visual and vestibular information. White noise ($\underline{W}_{rot}$) passes through a second order filter, with breakpoint (β_{rot}, to generate angular velocity (ω). Angular velocity is thus mathematically specified as a random process with a known bandwidth and rms value. Stated another way, the system does not know precisely what the angular velocity stimulus will be, but is expecting a certain spectrum. White noise is processed by a first-order filter, with breakpoint (β_{tran}) to generate translatory acceleration (acc), and ω and acc are both passed through first order filters with long time constants to approximate orientation angle (γ) and translatory velocity (vel) respectively. The integrations are "approximate" because pure integration of white noise leads to infinite covariance and makes Kalman gain calculation more difficult. Semicircular canals are assumed, by the internal model, to be driven by angular acceleration and otoliths by specific force as are the actual mechanisms. The visual system, on the other hand, is modeled as responding to angular and translational velocity since people seem to most readily interpret moving peripheral fields in terms of velocity. In each case, sensor dynamics consist of the linear part of the models reviewed in section 2.0 and thus the central processor is assumed to have fairly accurate knowledge of sensor function. Measurement noise is specified as a noise/signal ratio (ρ_i) which is multiplied by

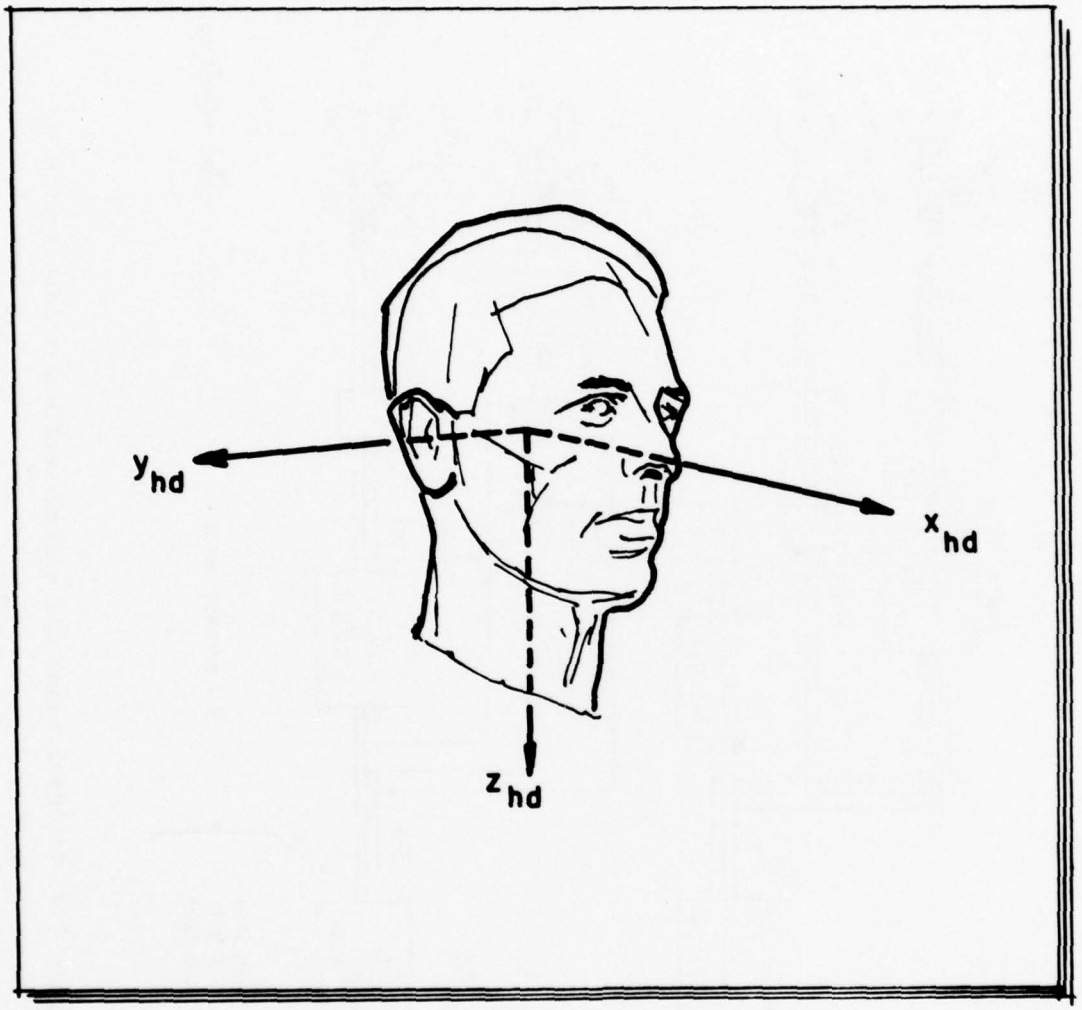

Figure 3.1 Head Coordinates

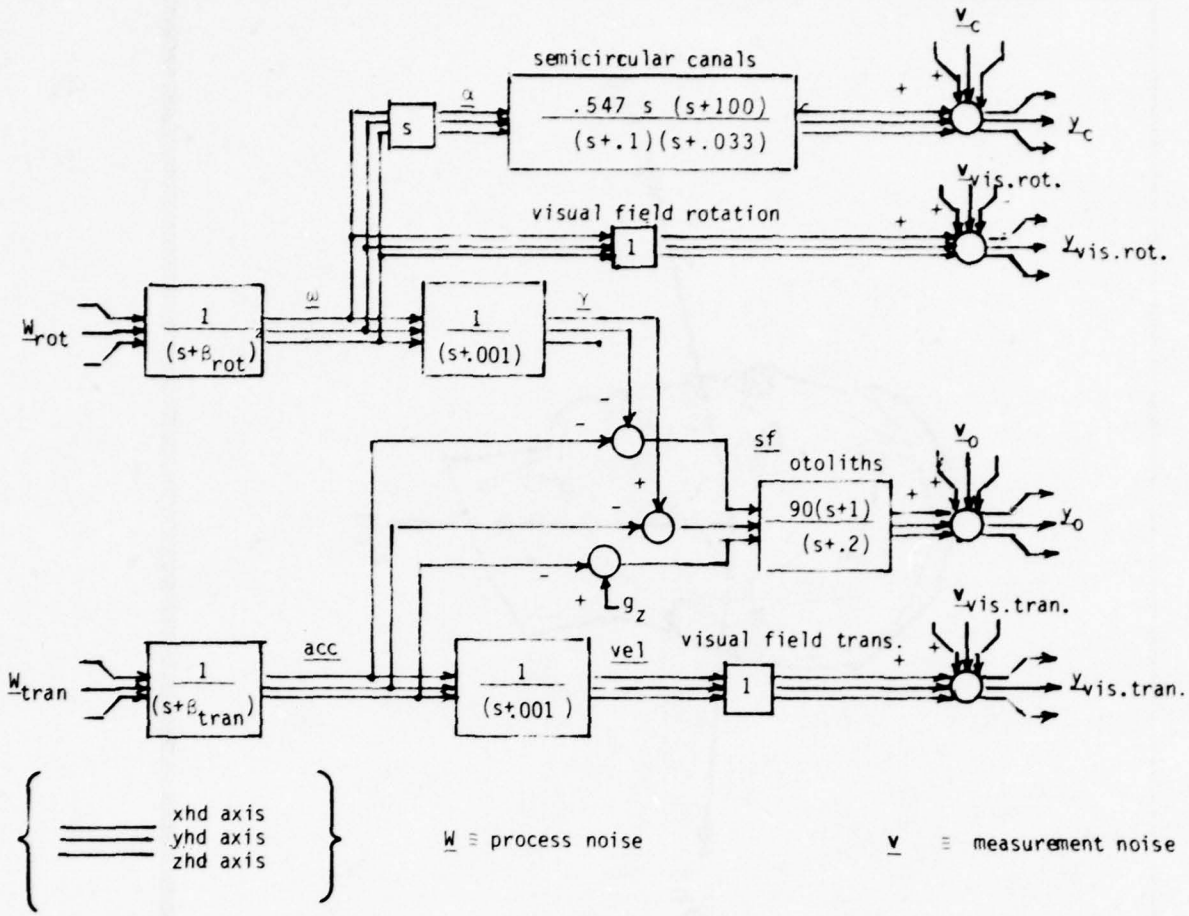

Figure 3.2 Internal model for visual-vestibular interaction

signal variance (σ_i^2) to form noise power spectral density.

Proprioceptive and tactile information is considered by using specific force channels in the internal model to drive the linear tactile and proprioceptive sensor dynamics discussed in section 2.0. Vestibular-tactile and vestibular-proprioceptive interactions have been tested in a preliminary way, using filters based on the internal model shown in Figure 3.3. Figure 3.4 shows an internal model that has been used to consider a visual horizon reference in addition to homogeneous field velocity.

The specific $\underline{W}$, $\underline{\beta}$, and $\underline{\rho}$ parameters used to generate the time responses presented later in this report are listed in Appendix C.

3.2 Input Spectra and Measurement Noise

There is no clear theoretical means for specifying the input spectrum. Perhaps it should be a typical spectrum associated with walking and running or perhaps a typical average aircraft flight spectrum, however, neither of the above is well known. In the case of a non-naive person (i.e., active pilot), the expected input spectrum probably changes continually to match the particular maneuver being initiated, as is discussed further in section 6.0. To find the stationary process that will yield the best results for the steady-state model, a nominal spectrum was gradually changed and adjusted to bring responses closer and closer to observed human response.

The most logical way to specify measurement noise might be to assume that the central processor has accurate knowledge of the noise associated with the information from each sensor; however, neurophysiological research has not yet unambiguously defined these values. Measurement noise ratios, as well as input spectra, have therefore been "tuned" to their present value. The system is quite sensitive to changes in both measurement noise and input spectrum and further tuning is expected to result in additional improvement.

3.3 Consideration of Sensor Threshold Effects

The interim report (1977) discusses use of random input describing functions (RIDFs) to approximate threshold effects in the internal model and thereby allow the Kalman filter to account for these effects in its estimates. A random input describing function is a linear gain which replaces the non-linearity and is chosen to minimize the mean squared error of the approximation. For a threshold

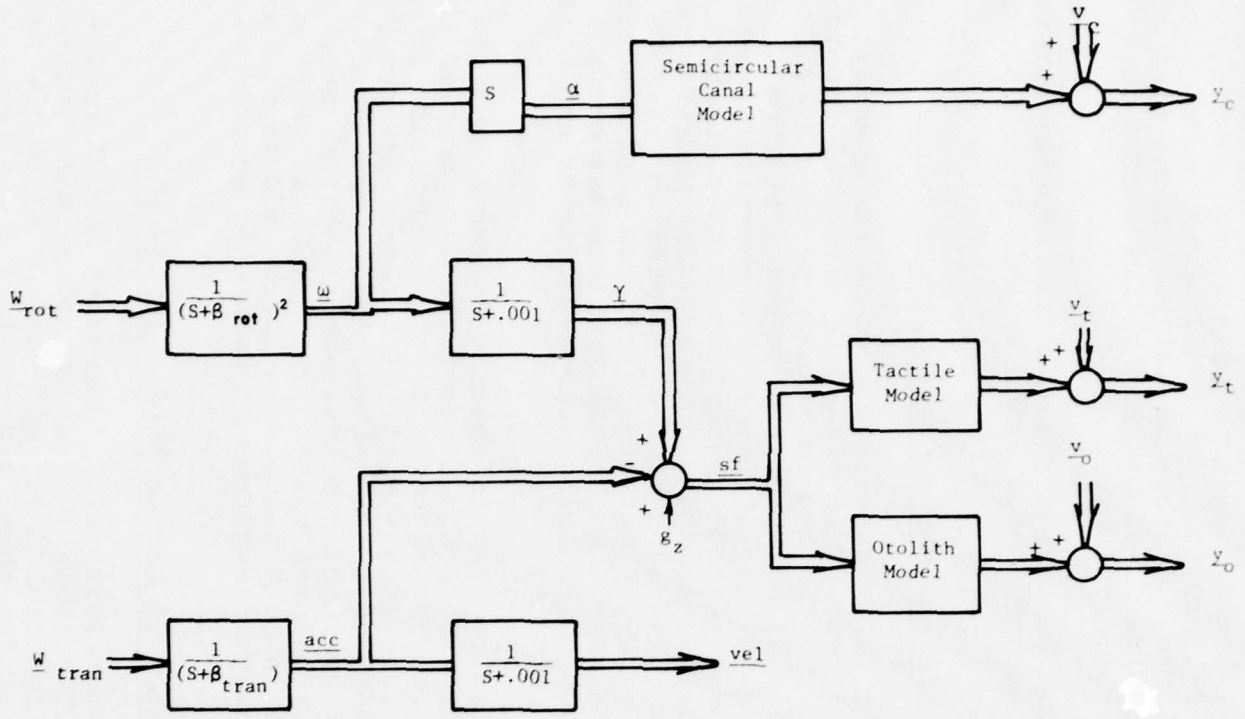

Figure 3.3 Internal model for tactile-vestibular interaction. "Canal", "otolith", and "tactile model" blocks contain the linear dynamics of figure 2.3, 2.4 and 2.6 respectively. For proprioceptive-vestibular interactions, the "tactile model" block is replaced by the proprioceptive head-neck model dynamics of figure 2.7

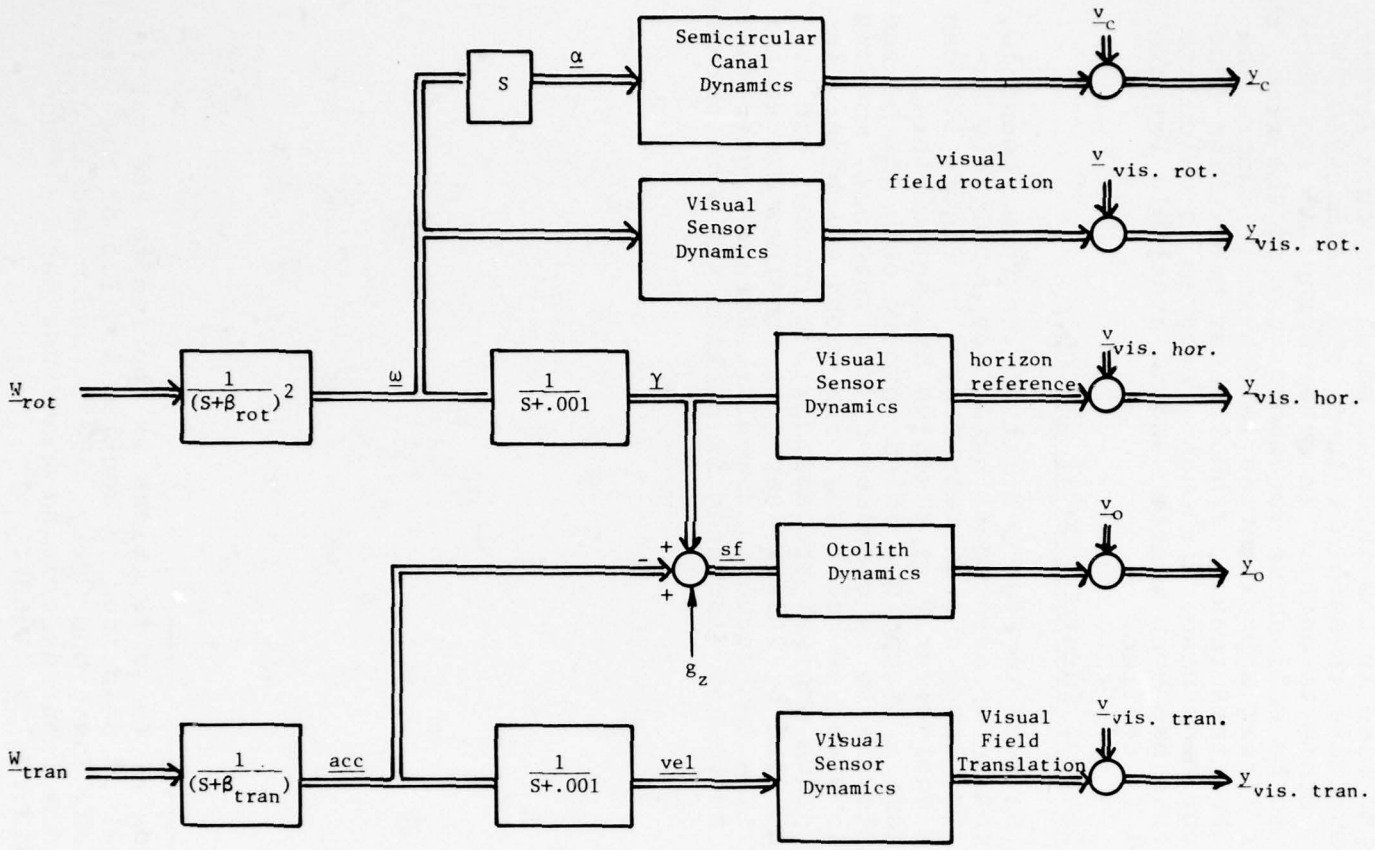

Figure 3.4 Internal model for visual-vestibular interaction with visual horizon reference included. Visual sensor dynamics are unity (see figure 2.5). Semicircular canal and otolith dynamics are the linear parts of figures 2.3 and 2.4 respectively.

non-linearity, it is a function of threshold value and the expected rms input to the threshold.* Currently, input variances specified in the internal model are much larger than the respective threshold values, and optimal RIDF gain is very close to unity. In other words, if the signal is expected to be well above threshold most of the time, the near-optimal linear approximation is to simply ignore the threshold. For this reason, random input describing functions have not been used, although a program to calculate these functions has been written and is available for use in the model if desired.

3.4 Decoupling of Internal Model Channels

It can be seen in Figure 3.2 that the three channels, each representing an orthogonal axis, are completely independent. The large system represented by Figure 3.2 can therefore be equivalently represented by a set of three smaller systems. If motions which involve only one of the three channels are to be considered (for instance, motions which only involve yaw rotation, or motions which only involve pitch plane motion) the appropriate channel can be decoupled and used by itself, saving a considerable amount of computer time and reducing computer storage requirements. Many of the responses discussed in section 4.0 were obtained in this way.

---

* Calculation of these functions as applied to the multisensory model is described in section 4.3.1.3 of the interim report (Borah, Young and Curry, 1977), and a detailed treatment of random input describing functions can be found in Gelb and VanderVelde (1968).

4.0 MODEL TIME RESPONSES WITH LINEAR CENTRAL PROCESSOR

The following model responses were obtained using a steady-state Kalman filter alone as the central processor. While it is recognized that this is not sufficient to predict all of the important characteristics of human motion perception, the steady-state filter alone has been successful to a surprising degree. Some necessary additions to the central processor are described in section 5.0.

The responses represent a naive subject who has no advance knowledge of the stimulus to be received or of the limits of his vehicle. The active pilot with varying skill levels and operating under different workloads is considered to be an extension of the more basic naive case, and means for extending the model to the active pilot are discussed in section 6.0.

4.1 Yaw Motion

Figure 4.1 shows several responses to combined visual field and platform rotation about the yaw axis. All curves, except the "CV" curve involve an inertial stimulus producing the semicircular canal afferent response shown in the figure. The afferent response curve is the output from the semicircular canal model and is one of the inputs to the central processor (see Figure 2.9).

When no visual information is present (in dense fog or in the dark, etc.) the model angular velocity estimate (curve labeled RD) shows the well documented adaptation to continuous rotation which proved to be such a problem for pre-instrument-era pilots. It is also significant that the decay in angular velocity perception lags behind that of the semicircular canal afferent response since this relation has also been observed experimentally.

When wide field visual information is present and is consistent with a physically stable visual surround, angular velocity perception is a fairly accurate reflection of true angular velocity as shown by the curve labeled RL. When the visual surround is fixed to the rotating platform so that the visual system always reports zero velocity, the curve labeled RFF shows an adapting response similar to the case of rotation in the dark (RD), but with a smaller magnitude and faster adaptation constant. The RFF curve makes intuitive sense since the visual surround is actively "denying" the presence of motion not just failing to provide information. In most cases, however, experimental observations have not provided enough evidence to clearly distinguish between the dark (RD) and vehicle fixed field (RFF)

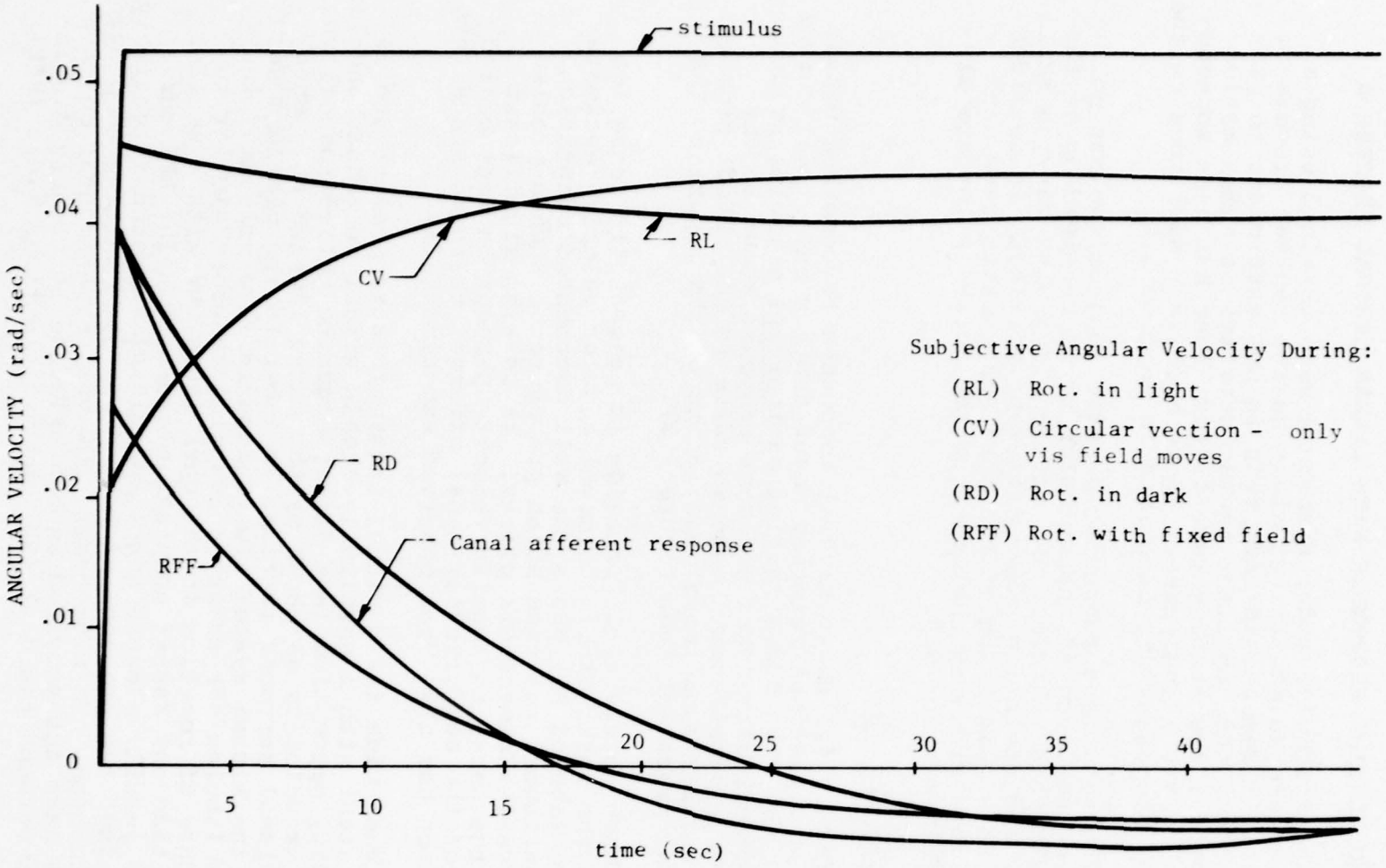

Figure 4.1 Model response to combined platform and wide visual field yaw motion.

situations; and in some cases, RFF appears to be the stronger response, especially for very low accelerations in which the oculogyral illusion, present for RFF, strengthens the near threshold response.

When the platform is stationary and the visual surround rotates, as for instance in a fixed-base simulator with a wide visual field display, the curve labeled CV shows a gradual onset of angular velocity sensation over a period of about 10 seconds. This is a classical circularvection (visually induced rotation) response with one important exception. The exponential onset of sensation is shown to begin immediately after the onset of visual field motion whereas a delay is often observed in human response. The onset delay appears to be a highly variable and non-linear phenomenon which cannot be produced by the steady-state Kalman filter alone, but has been created with the addition of a non-linear model element as described in section 5.0.

RL, RFF, and CV curves were generated using a steady-state Kalman filter derived from the internal model of Figure 3.2. Since the system does not expect visual information during rotation in the dark, Kalman gains for the RD curve were calculated by deleting visual channels from Figure 3.2. An equivalent strategy would be to use an extremely high visual channel noise ratio in the internal model.

The rotational stimulus shown in Figure 4.1 was applied to both visual and vestibular components of the time history program (see Figure 2.9) to produce the RL response, while the RFF and CV responses were produced by substituting zero inputs to the visual and vestibular sensors respectively. (The vestibular sensors cannot be turned off.) In the case of the RD curve, input to the visual model is irrelevant since the central processor is unaware of visual information, and so, the visual channel is opened.

Except for the absence of a circularvection onset delay, the relations between the various curves of Figure 4.1 are quite similar to those observed experimentally.

4.2 Forward Acceleration

Forward acceleration is detected by the otoliths as an elongation and rotation of the specific force vector while the canals continue to signal zero rotation. When visual information is unavailable (in dense fog or in the dark, etc.), the model predicts an initial translatory acceleration sensation that is gradually replaced by a pitch-up illusion, as shown in Figure 4.2. Stated another way, the

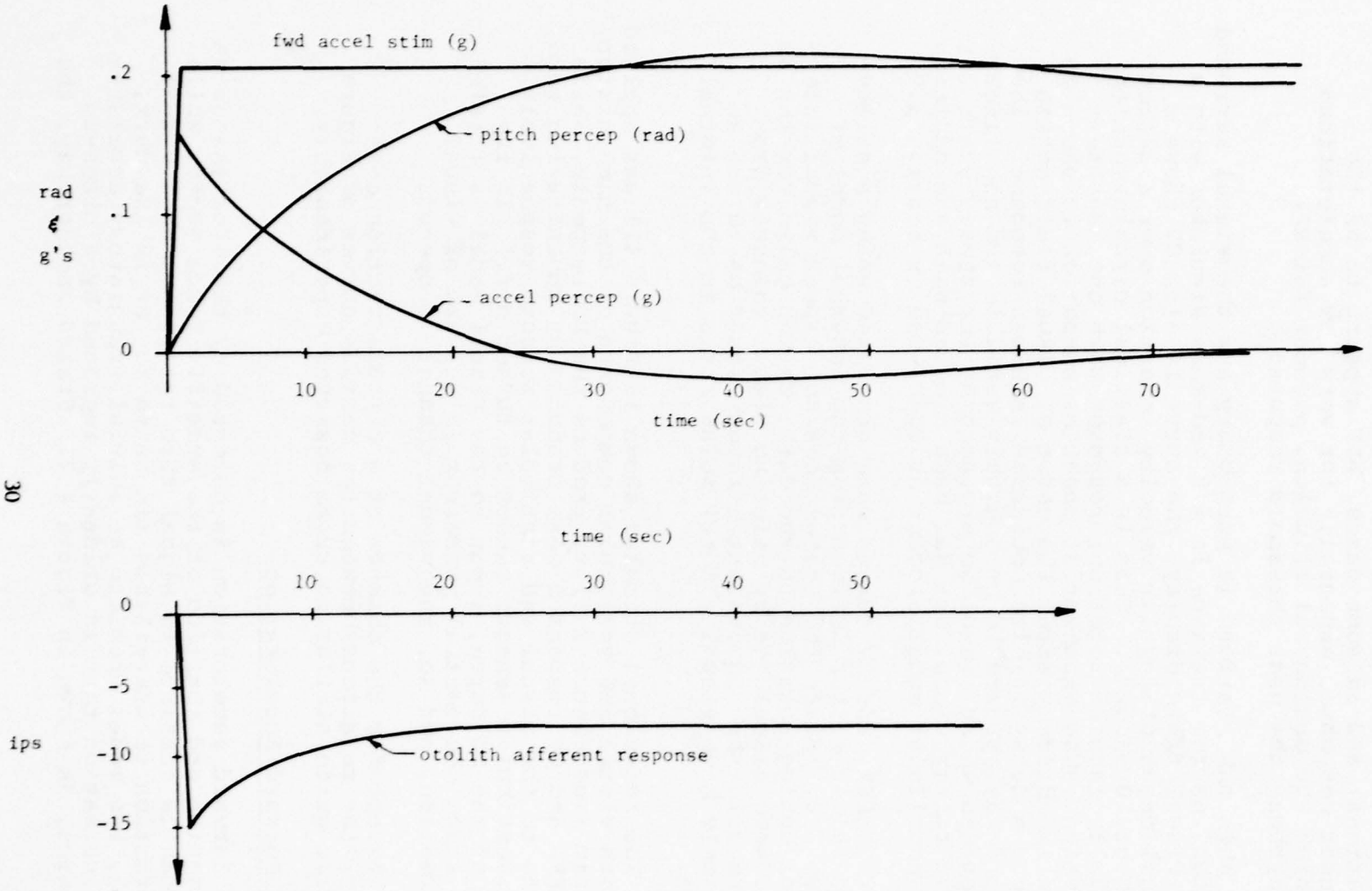

Figure 4.2 Model response to forward acceleration "in the dark" (vestibular cues alone)

system assumes that, in the steady-state, specific force is approximately aligned with gravity. This is qualitatively consistent with the well documented pitch illusion experienced by pilots during aircraft catapult launch. The steady-state alignment of perceived "down" with the specific force vector is confirmed by a centrifuge experiment performed by Wolfe and Cramer (1970). Centrifuge simulation of a catapult launch profile by Cohen et al. (1973), during which subjects attempted to keep a target at subjective eye level, suggests a time constant of 40-60 seconds for the illusion, and a centrifuge experiment by Graybiel & Brown (1951) shows a 60 second settling time. The Wolfe and Cramer (1970) results, on the other hand, imply a much more rapid manifestation of the illusion, although their experiment was *not* specifically designed to study onset dynamics. Additional data would be useful to more conclusively document the pitch illusion time course.

When confirming visual information is present in the form of a moving homogeneous peripheral field, the model predicts a relatively accurate interpretation of the stimulus. If output of the visual sensor is restricted by a saturation limit (see visual sensor model in Figure 2.5), the model yields an accurate estimate of the stimulus until the visual limit is encountered, at which point the pitch illusion returns. Both cases, with and without visual saturation, are shown in Figure 4.3. The visual cues considered in the above examples contain only velocity and no steady-state orientation or position information. If a visual horizon reference is also included (see internal model of Figure 3.4), the model predicts less pitch illusion even after the visual field velocity limit is exceeded, and this is shown in Figure 4.4. As confidence in the horizon reference increases, modeled by a smaller measurement noise ratio in the internal model, the predicted pitch illusion diminishes still further.

Figure 4.5 shows the velocity sensation predicted by the model for all acceleration stimuli so far discussed. All responses are as expected except for the case of acceleration "in the dark." The absence of significant steady-state velocity perception is reasonable in this response since the stimulus is eventually interpreted as a pitch-up rather than a forward acceleration. It seems unlikely, however, that the human will not initially experience a significant sensation of increasing velocity if accelerated under similar conditions. No explicit data are currently available against which to match this response but the situation warrants further exploration.

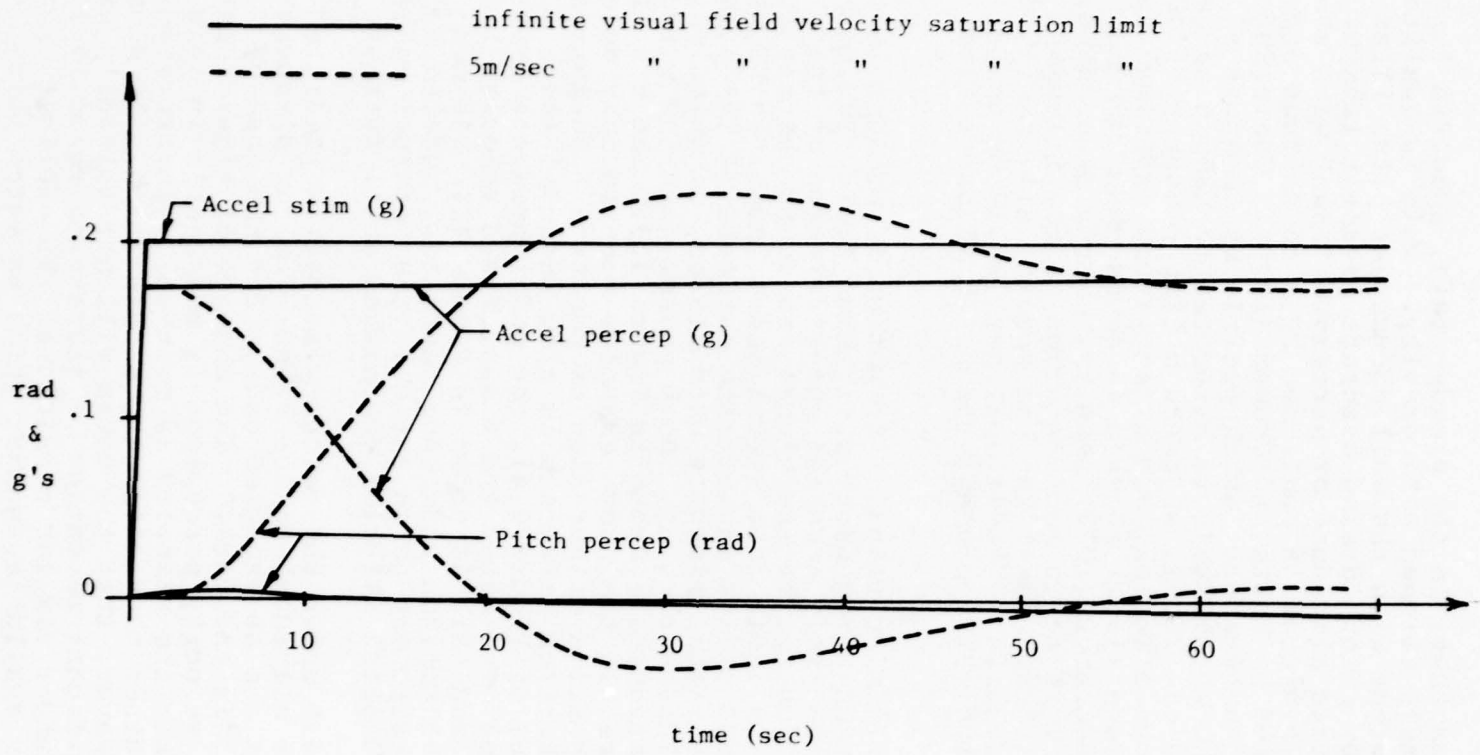

Figure 4.3 Model Response to Forward Acceleration with Confirming Visual Field Velocity Cues

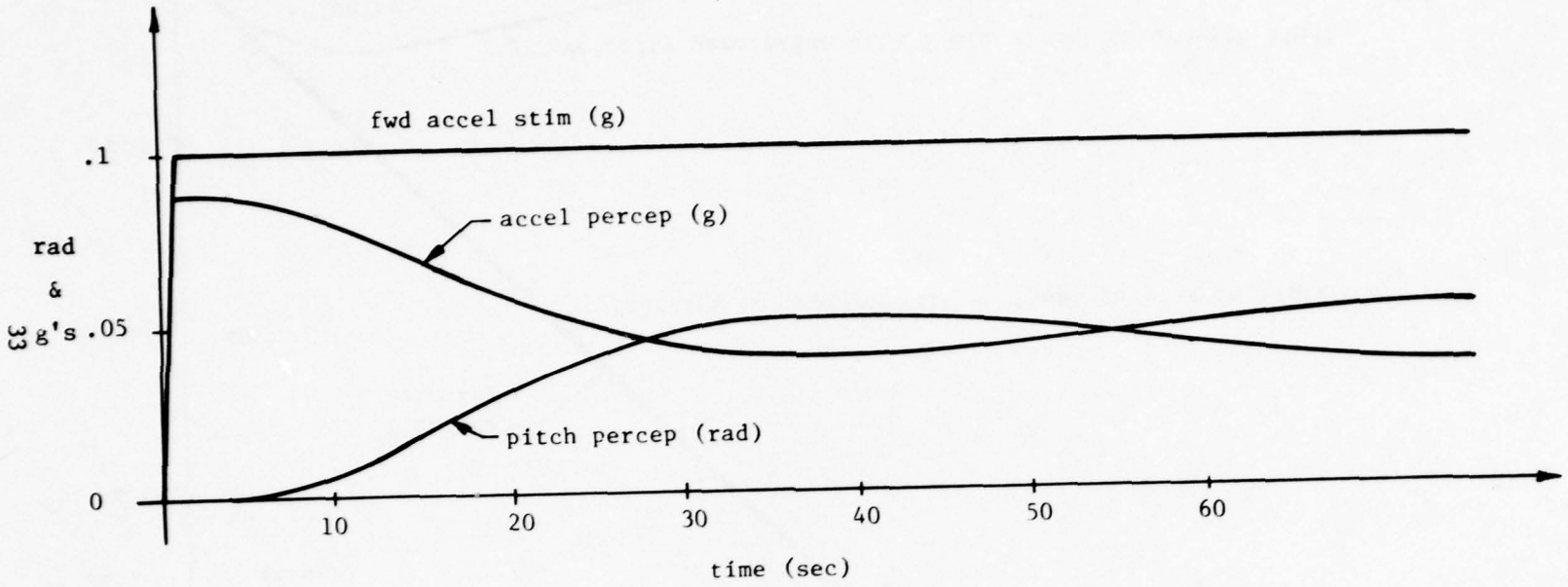

Figure 4.4 Model Response to Forward Acceleration with Confirming Visual Field Velocity cues, 5 m/sec visual saturation limit, and a visual horizon reference

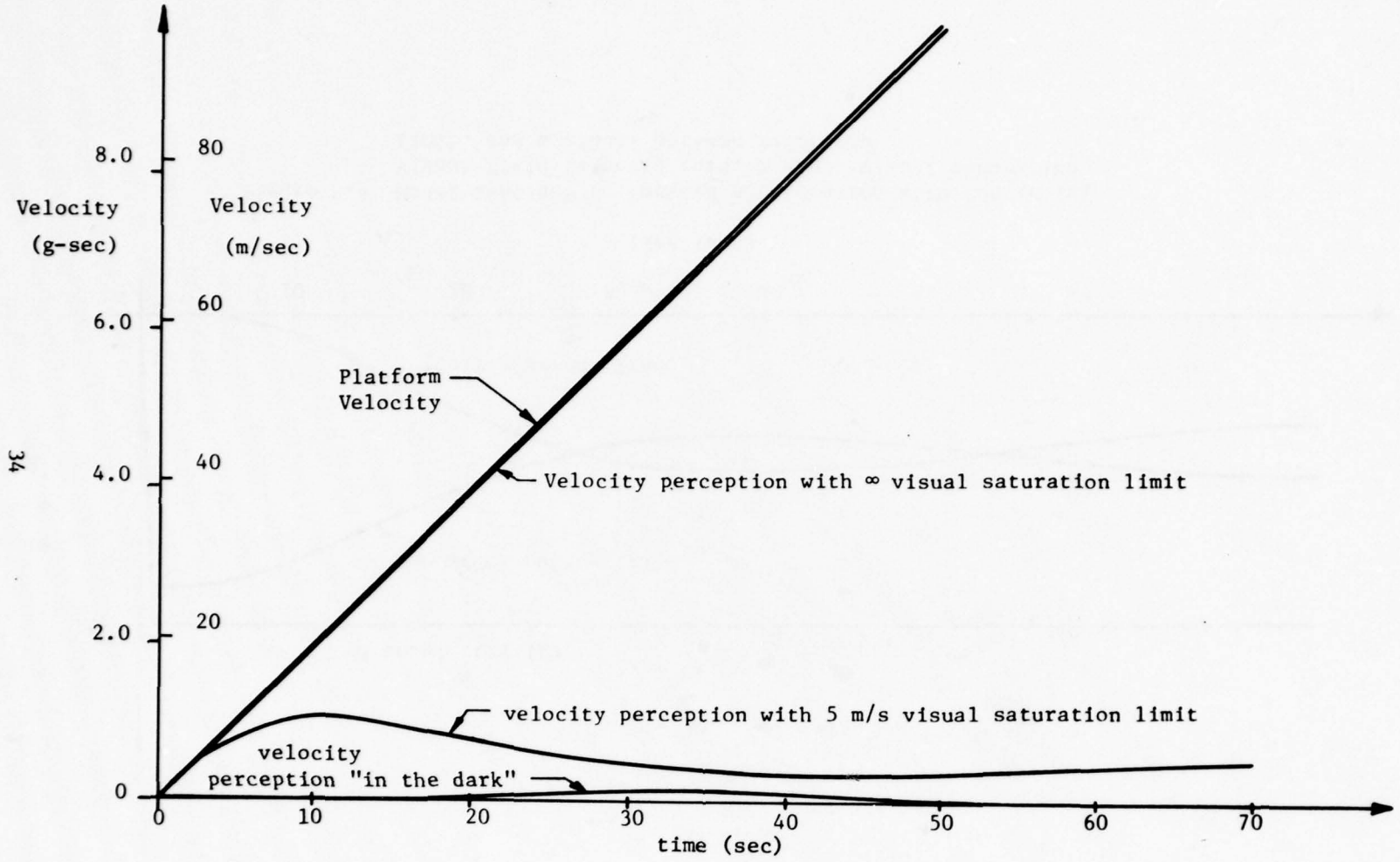

Figure 4.5a Velocity perception during forward acceleration

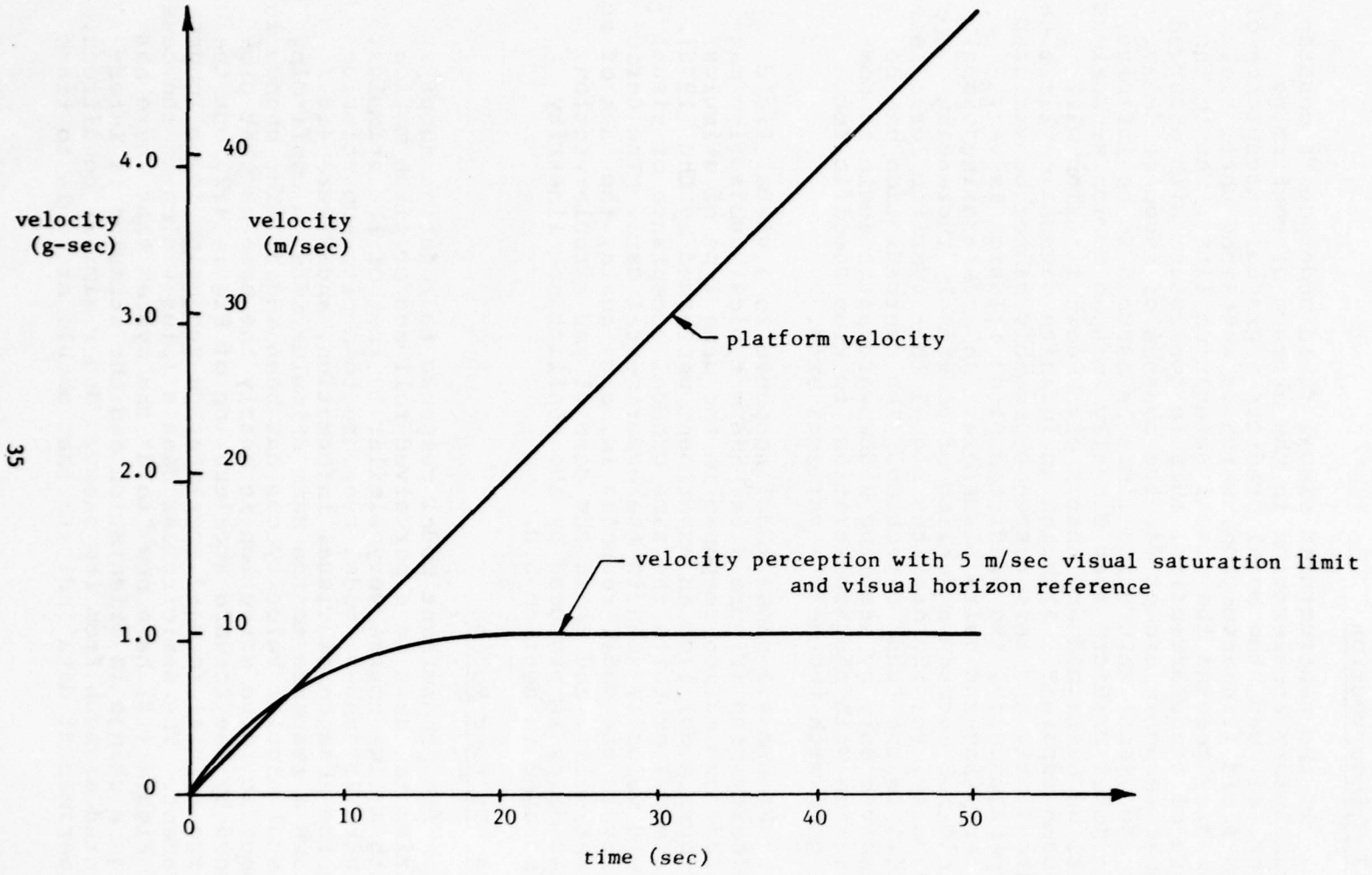

Figure 4.5b Velocity perception during forward acceleration

4.3 Linearvection

If the unstructured visual field undergoes a constant translatory acceleration in the absence of confirming inertial cues, the model predicts a gradual acceptance of the field (linearvection) which is sustained until field velocity reaches the visual saturation limit. As in the case of circularvection, this is consistent with observed human response except for the absence of response delay. If the visual saturation limit is assumed to be infinite, the model predicts that visually induced motion sensations will be sustained and that a pitch-down illusion will become apparent. Although an infinite saturation limit is unrealistic and this response probably cannot be verified experimentally, the predicted pitch illusion is very interesting and quite plausible. An accelerating visual field has induced a feeling of constantly increasing velocity, yet the otoliths signal that specific force is still in the "zhd" direction. The contradiction can be resolved only by assuming a downward pitch angle in combination with the acceleration, to keep specific force aligned with the head's vertical axis.

Figure 4.6 shows model response to a visual field velocity step (Figure 4.6a) and a typical subjective magnitude estimation response to the same type of stimulus (Figure 4.6b) from an experiment performed by Chu (1976). The model exhibits the same gradual acceptance of visual field velocity seen in the experimental data. The deficiency in the model response is, once again, the lack of an onset delay, and as in the case of yaw circularvection, this delay is produced by the conflict non-linearity discussed in section 5.0.

4.4 Tilting Motion

The predominant model response to rotation about a horizontal axis is a perceived roll and/or pitch motion with a time course very similar to that of the stimulus. Figure 4.7 shows model response to a pitch-up stimulus in the absence of visual information, and Figure 4.8 shows a response to the same stimulus after a confirming visual angular velocity cue has been added. The change in specific force direction is nearly the same as that produced by the forward acceleration of Figure 4.2, but the large initial forward acceleration sensation is no longer present. The semicircular canals (plus vision in the case of Figure 4.8) have now "told" the system that there has been a change in orientation and the stimulus is interpreted as such from its onset. Under similar conditions, experimental data indicate that people are able to track

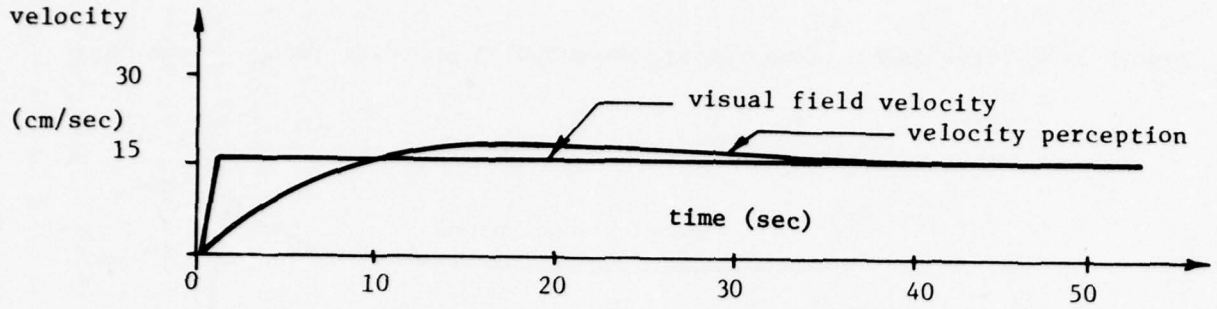

a. Model Linearvection Response

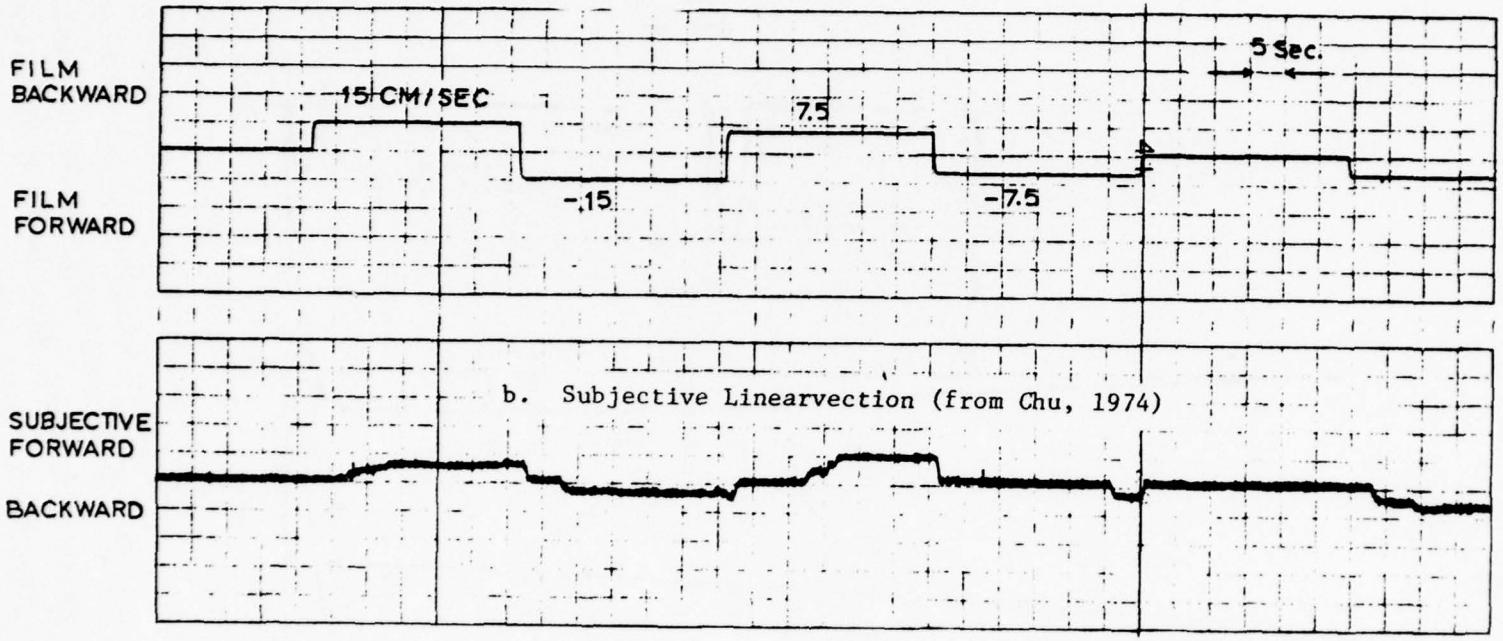

b. Subjective Linearvection (from Chu, 1974)

Figure 4.6 Linearvection

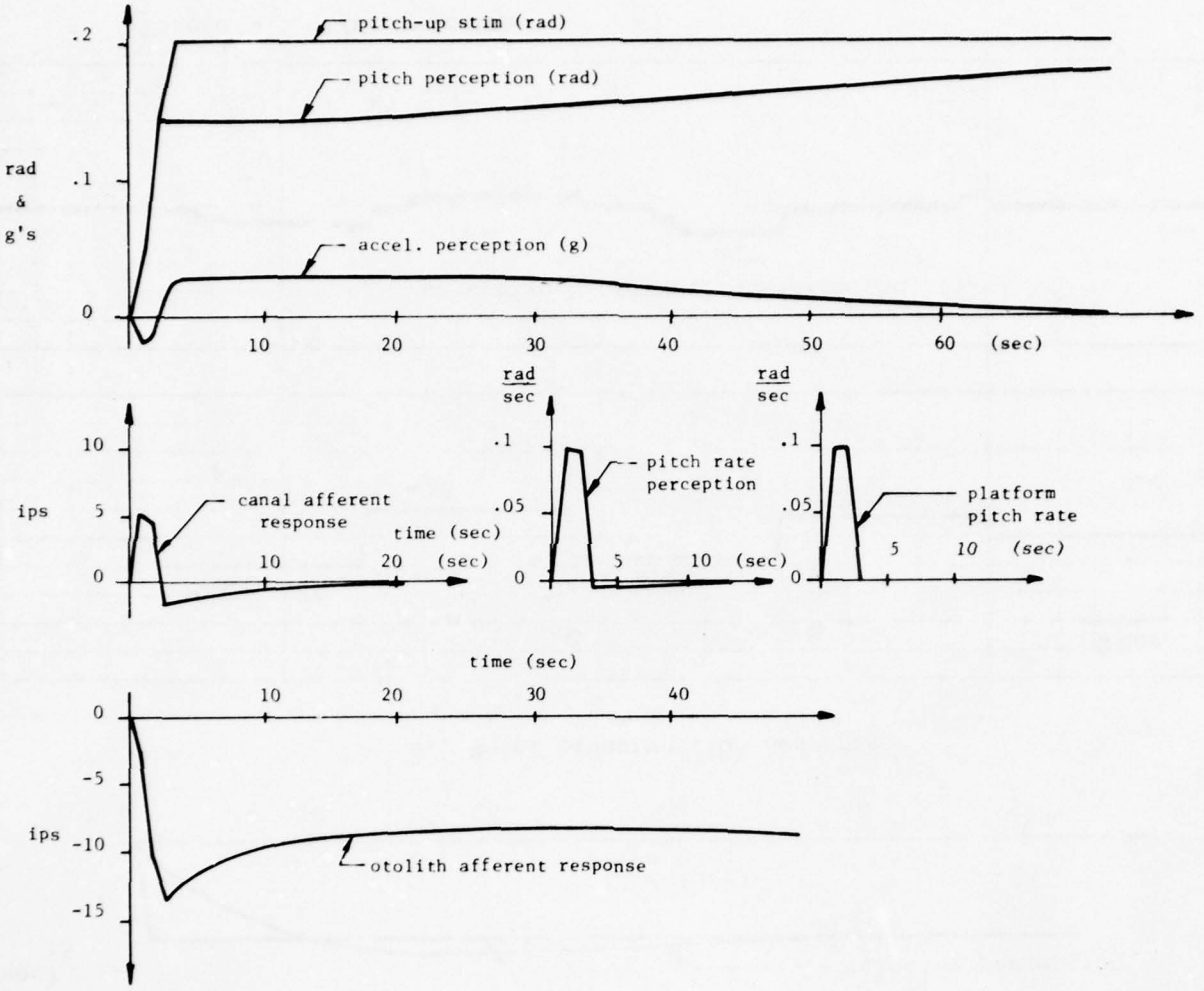

Figure 4.7 Model response to pitch-up "in the dark" (vestibular cues alone)

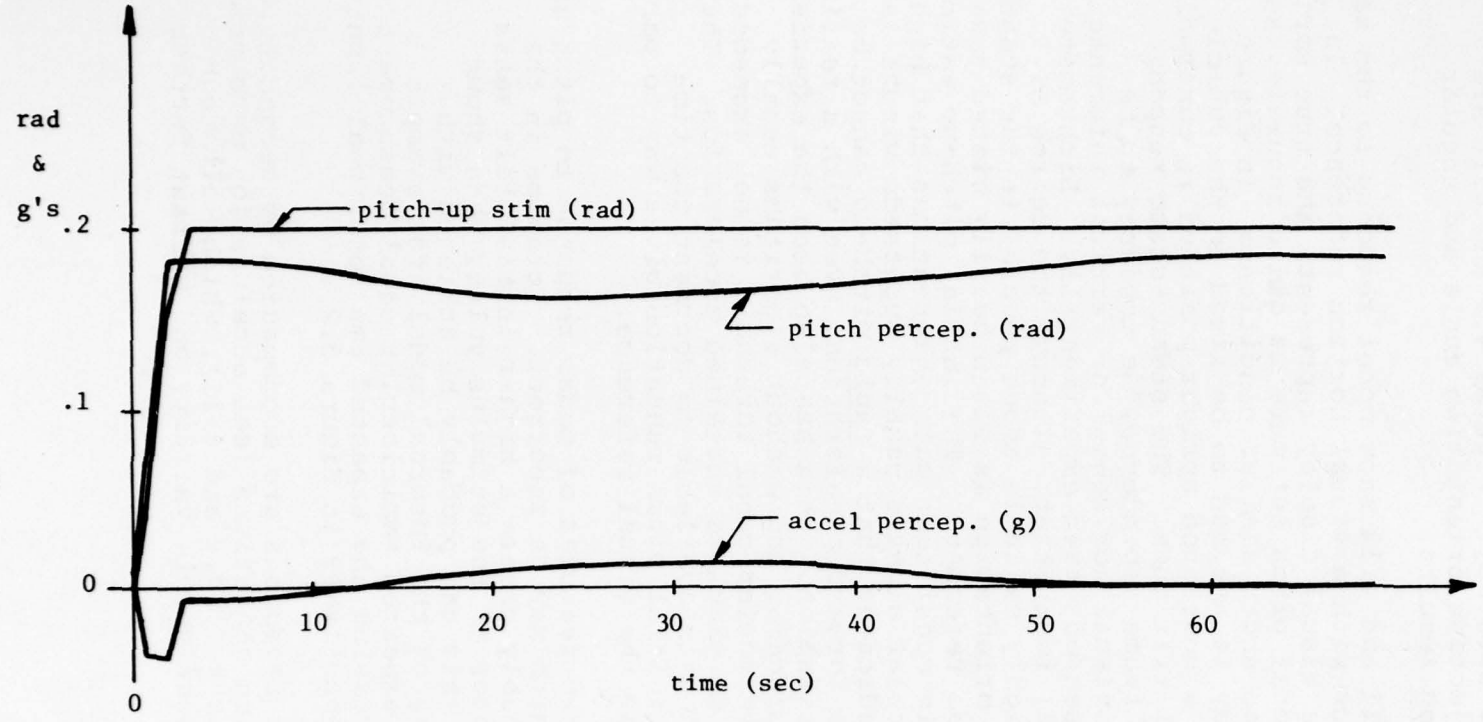

Figure 4.8 Model response to pitch-up with confirming visual field angular velocity cue

both angular velocity and changes in their orientation with a fair degree of accuracy. Figures 4.9 and 4.10 are examples of subjective orientation angle and angular velocity tracking results.

Figures 4.11 and 4.12 show model response to the same pitch-up stimulus with a visual horizon reference. In Figure 4.11, the visual display represents the true horizon position, and model pitch estimate is quite accurate, as is human response under similar conditions. In Figure 4.12, the display is assumed to be fixed to the vehicle so that it signals a continued upright position in contradiction of inertial tilt cues. The steady-state response shows a visual "frame dependence," a tendency to be influenced by a visual horizontal or vertical reference, that has also been observed experimentally. Lichtenstein and Saucer (1972) found that, although the degree of dependence is highly variable among people, in the steady-state perceived orientation is often heavily biased towards a visual attitude reference. The initial pitch-up estimate in Figure 4.12 is consistent with observations that high frequency vestibular signals usually supersede visual information and indicates that a rapid pitch-up cannot be used to simulate forward acceleration, even with a realistic visual presentation. This has also been the experience of simulator designers, and washout algorithms usually ensure that semicircular canal threshold is not exceeded when using tilt to simulate sustained acceleration. There are currently no data available to document the time course by which initial pitch sensation gives way to partial acceptance of the visual reference.

There are two features of model response to pitch and roll rotation which may be incorrect. Rotation in the dark should probably create a higher initial tilt sensation, coming closer to the stimulus value, than shown in Figure 4.7. This can probably be achieved with additional tuning of the internal model, for example, by lowering the expected semicircular canal measurement noise or by increasing the expected rms rotational input (V_c and W_{rot} respectively in Figure 3.2).

Model pitch responses are accompanied by secondary translatory motion sensations (see acceleration perception curves in Figures 4.7, 4.8 and 4.11), which, although small, are of questionable validity and warrant further investigation.

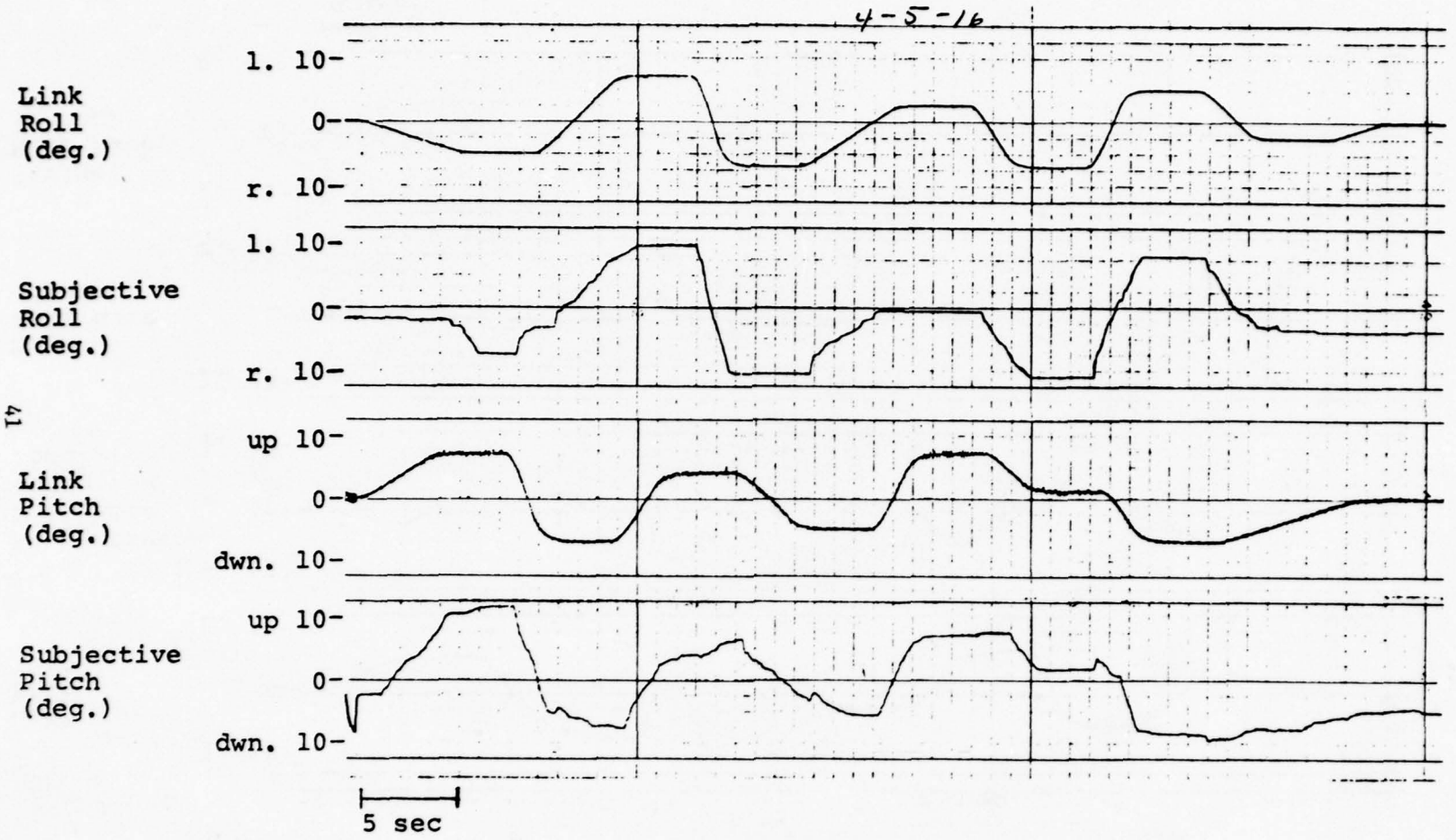

Figure 4.9 Typical results from subjective orientation angle tracking task in a Link trainer. Subject was attempting to keep a pointer earth vertical. (From Borah, 1976).

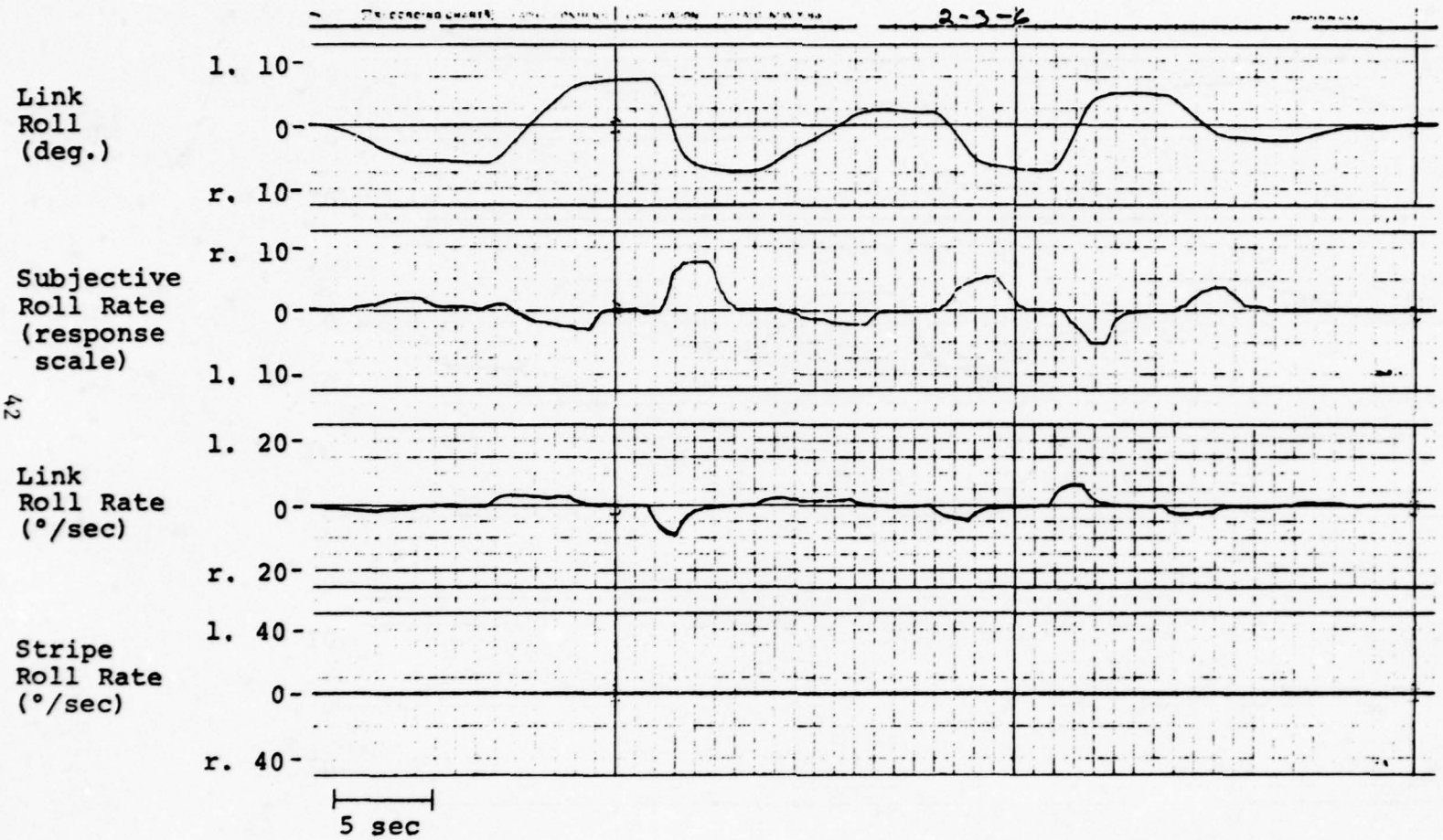

Figure 4.10 Subjective roll velocity magnitude estimation in a Link trainer. (From Borah, 1976).

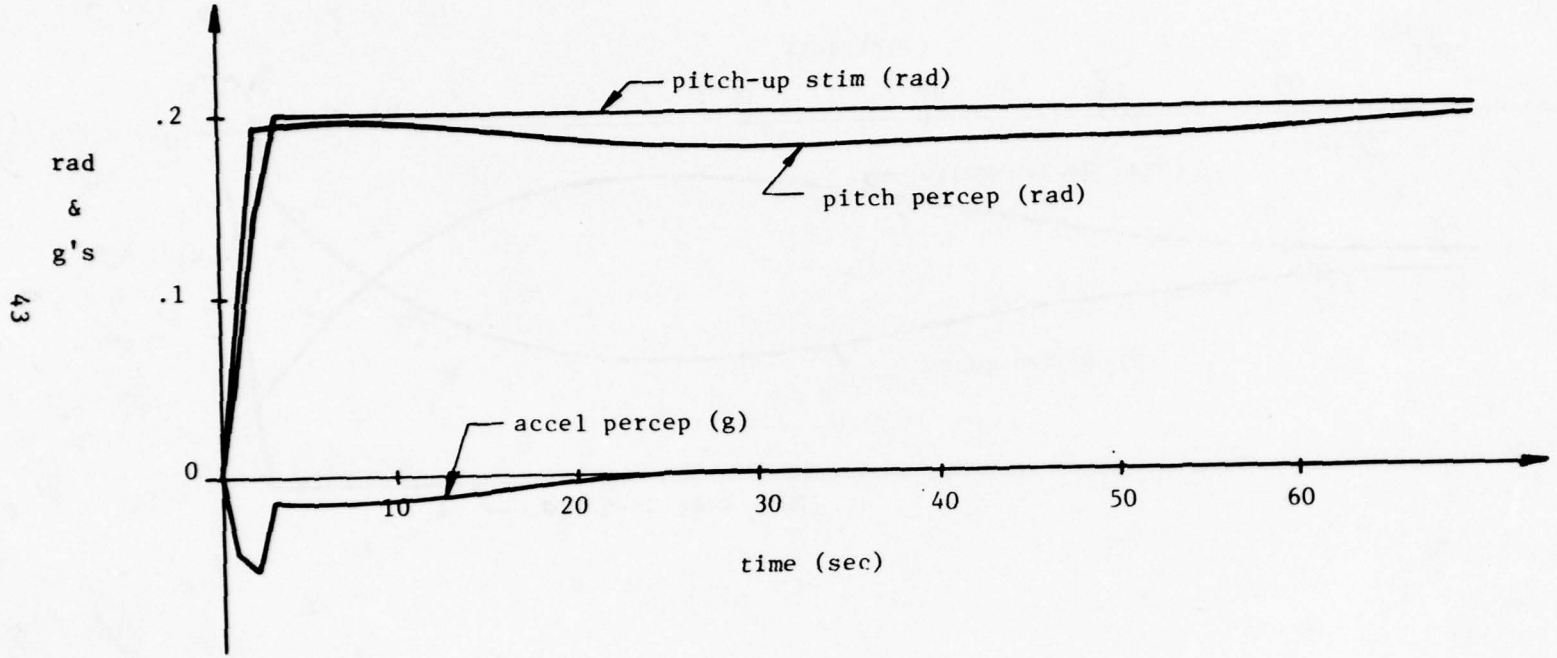

Figure 4.11 Model response to pitch-up with confirming visual horizon reference

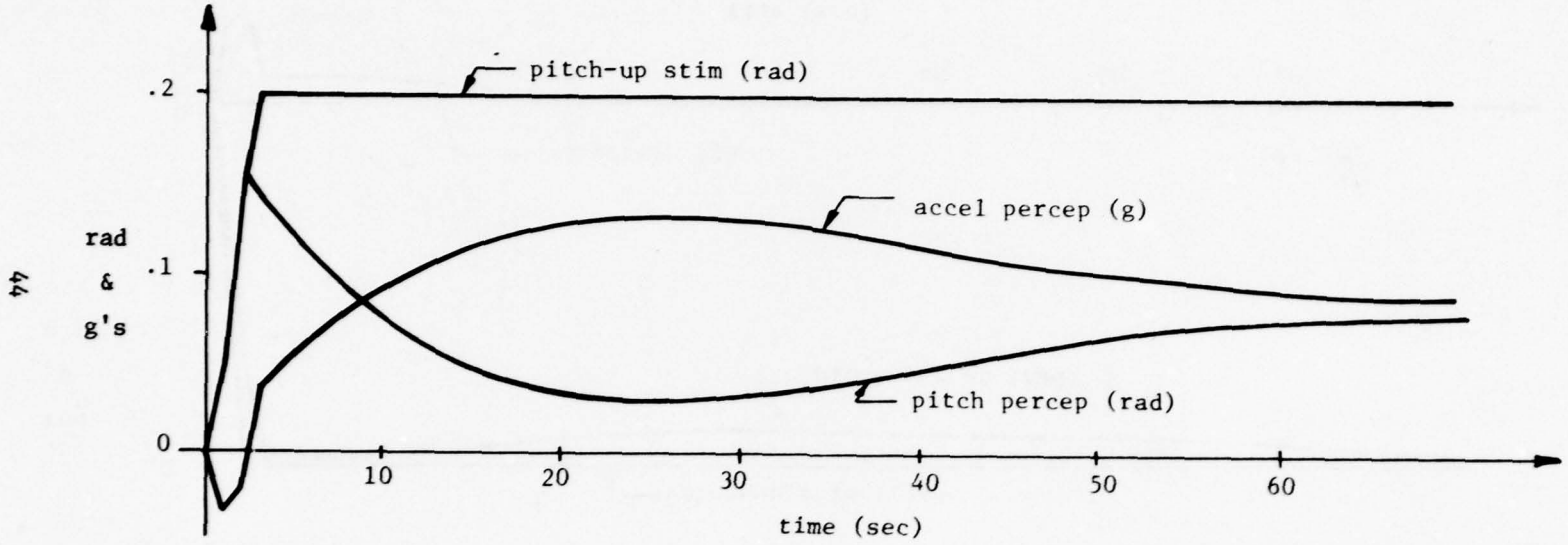

Figure 4.12 Model response to pitch-up with vehicle-fixed visual horizon reference

4.5 Response to Tactile and Proprioceptive Input

Preliminary exercise of tactile and proprioceptive model components has yielded responses which appear to be quite reasonable. Figure 4.13 contains an example of combined vestibular-tactile response to a forward acceleration signal. When tactile and vestibular cues are confirming, as they are during a real forward acceleration, the response is almost identical to that of the vestibular system alone. Since both otoliths and tactile sensors respond to the specific force vector, the tactile system is adding little new information and the response makes good intuitive sense. If only the tactile system is stimulated as though a very realistic g-cueing seat is being used on a stationary platform, the model predicts a sensation with a similar time course but a reduced magnitude. This is also logical considering that a nearly zero signal is being received from the vestibular system contradicting the tactile cue.

Figure 4.14 shows combined head-neck proprioception and vestibular model response to a lateral acceleration. The result is very similar to tactile-vestibular response and appears sensible for the same reasons. Truly meaningful evaluation of tactile and proprioceptive components, however, will require supportive psychophysical data as yet unavailable. Some of the experiments suggested in section 7.0 will enlarge the data base in this area.

4.6 Summary of Model Time Responses

The multi-sensory model, using a linear estimator alone as central processor, is in good agreement with the following characteristics of human motion perception:

- Decay of yaw velocity sensation during constant velocity yaw rotation, in the absence of visual cues.
- Relatively accurate yaw velocity sensation in the presence of confirming visual cues.
- Gradual acceptance of visual field rotation velocity (circularvection) about a vertical axis, in the absence of platform motion.
- Gradual illusion of pitch-up during prolonged or very large forward acceleration such as commonly experienced by aircraft carrier pilots during catapult launch.
- Fairly accurate perception of forward acceleration in the presence of confirming visual cues.

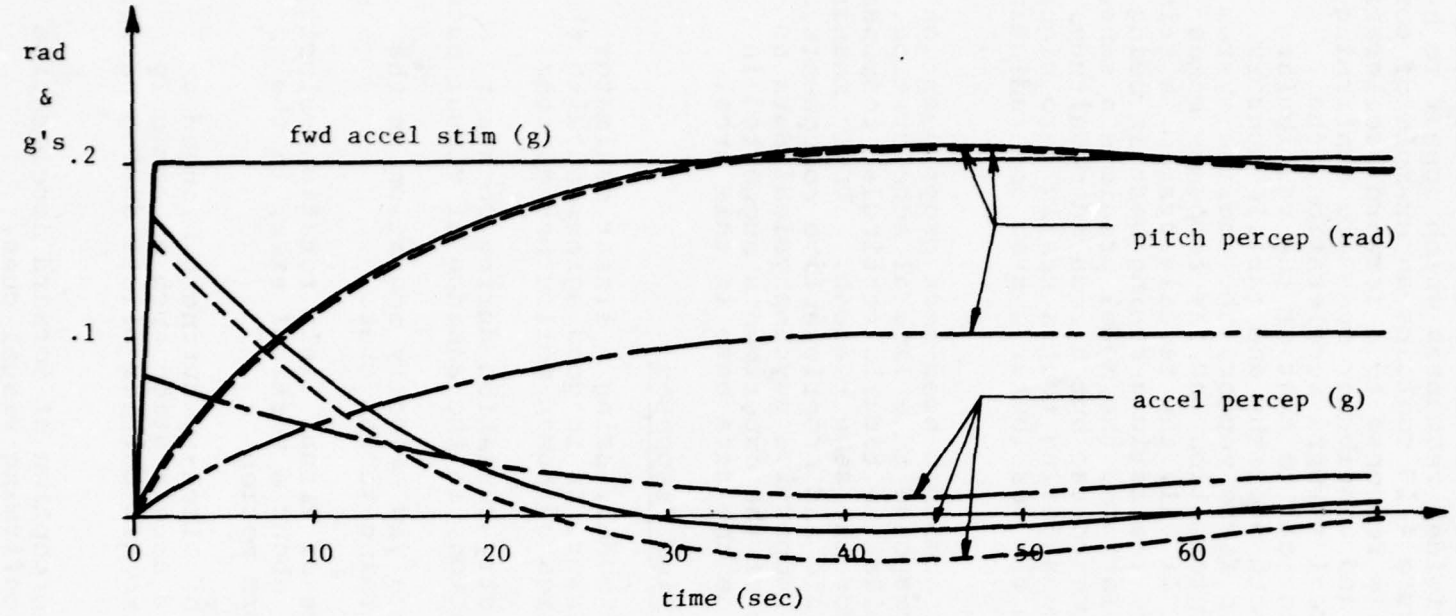

confirming tactile & vestibular cues

model containing only vestibular component

g-cueing seat stimulation on stationary platform

Figure 4.13 Tactile-vestibular model response to forward acceleration

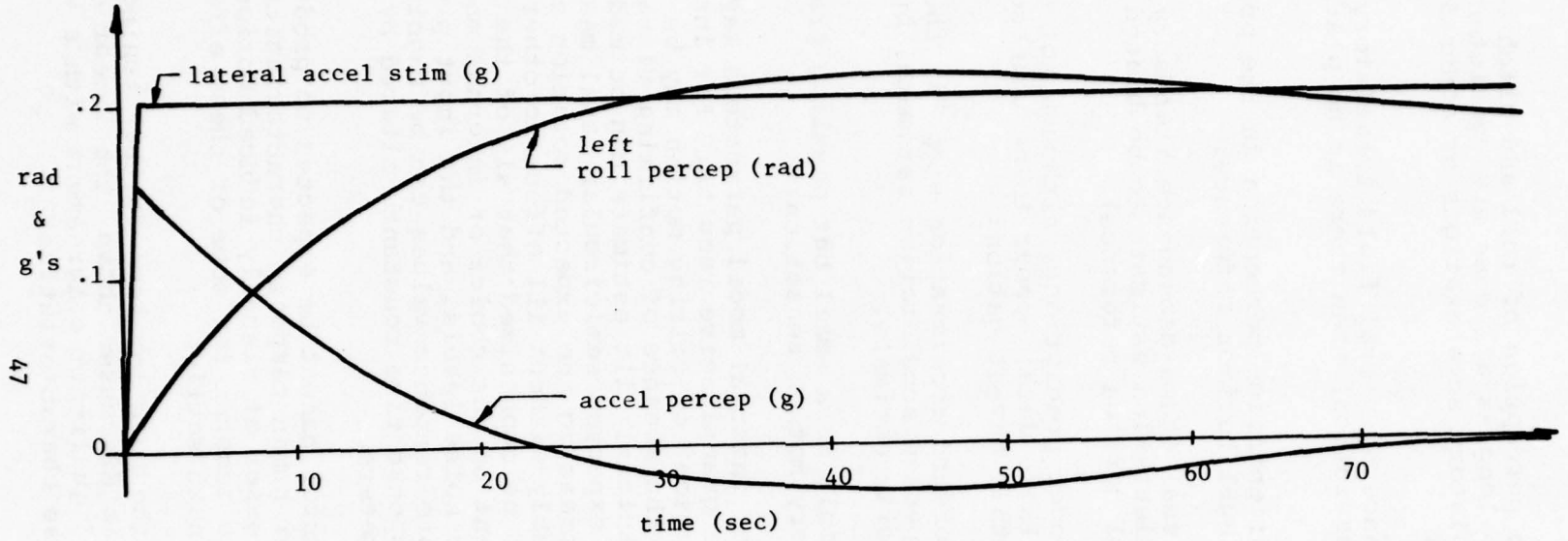

Figure 4.14 Proprioceptive-vestibular model response to lateral acceleration. Note that left roll has been drawn with positive values (contrary to "right hand rule" convention to facilitate comparison of this figure with forward acceleration responses.

- Fairly accurate perception of roll and pitch orientation changes so long as all cues are consistent (i.e., no translatory accelerations or contradictory visual stimuli)

- Gradual acceptance of visual field translatory velocity (linearvection) when there is no platform motion.

- Very accurate orientation perception in the presence of a correct visual horizon reference.

- Steady-state visual frame dependence (tendency for steady-state orientation estimate to be biased by incorrect visual horizon reference).

The following model predictions, although not directly contradicted by available data, appear to be unreasonable and require some further investigation:

- A translatory forward acceleration step "in the dark" produces the expected acceleration estimate, but a negligible velocity estimate.

- Tilt motions result in a small but puzzling prediction of translatory motion sensation.

Further tuning of internal model parameters may be needed to adjust some quantitative results. For instance, initial model "perception" of tilting motion may be too small, especially in the absence of confirming visual cues (Figure 4.7). This initial tilt estimate can be made larger by decreasing expected semicircular canal measurement noise and/or increasing the expected rotation channel input variance, probably without ill effect to other responses. It should be emphasized that all of the model responses are dependent on the choice of internal model input and measurement noise levels, and the input process spectrum. Steady-state response values can be magnified or attenuated and response time constants altered by adjusting these parameters.

The linear estimator cannot be expected to produce some highly non-linear human response characteristics, such as the delay in onset of visually induced motion, and model additions to account for some of these effects are described in the next section.

Notwithstanding the need for some further tuning and non-linear additions as discussed above, the linear estimator alone shows good qualitative agreement with a wide range of human response characteristics.

5.0 NON-LINEAR ADDITIONS TO THE MODEL

5.1 Cue Conflict Non-Linearity

The onset of visually induced motion sensation has been observed to occur only after a highly variable delay which is a function of mental set, compelling nature of the display, and stimulus magnitude. For modeling purposes both a favorable mental set and a compelling display are assumed. Given these conditions, the onset delay is often undetectable when visual stimulus magnitudes are near vestibular thresholds and becomes larger as the visual stimulus exceeds these values. The onset delay also vanishes in the presence of confirming vestibular cues of sufficient magnitude.

Figure 5.1 shows a generalized cue conflict scheme adapted for use with the Kalman filter estimator from a conflict model developed by Zacharias and Young (1977). Visual information is used to estimate expected vestibular response and then compared to actual vestibular response. The resultant error signal is rectified and passed through an adaptation operator so that any sustained errors will eventually be "washed-out." A switch keeps visual gain (K) at unity so long as the rectified, "washed-out" error is small and gradually drops the gain to zero as this error approaches vestibular threshold value (ε).

Figure 5.2 shows the response of the combined linear central processor and cue conflict element to a series of steps in visual field yaw velocity, all beginning at t=0. Responses now show an onset delay which increases with stimulus magnitude as found experimentally. The presence of the conflict non-linearity affects only the circular-vection (CV) response in Figure 4.1. When both the visual and vestibular systems are stimulated (RL curve of Figure 4.1), the conflict is zero and visual gain (K) remains unity. In the other two stimulus combinations presented in Figure 4.1, the visual signal is either zero (rotation with a vehicle fixed visual surround) or non-existent (rotation in the dark), and the value of K is, therefore, irrelevant.

5.2 Large Angle Correction

The internal model is linearized about a 1g upright orientation. At large tilt angles or during very large accelerations, errors introduced by the inherent small angle assumptions appear in the linear filter estimates. Specifically, static pitch and roll estimates are proportional to specific force along the head x and y axes ($\theta \simeq \sin\theta$). Model output can be corrected for large angles,

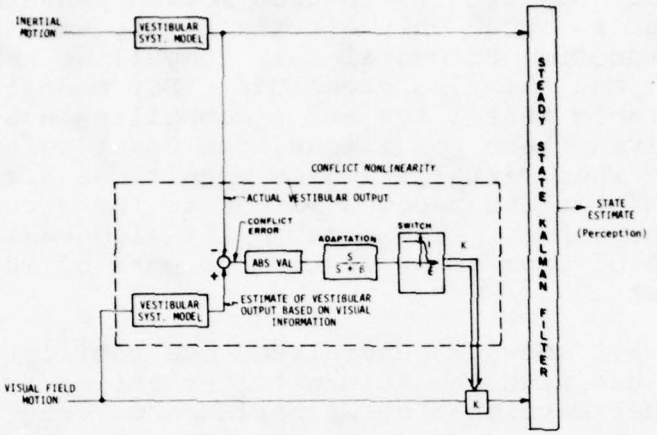

Figure 5.1 Conflict non-linearity combined with Kalman filter model

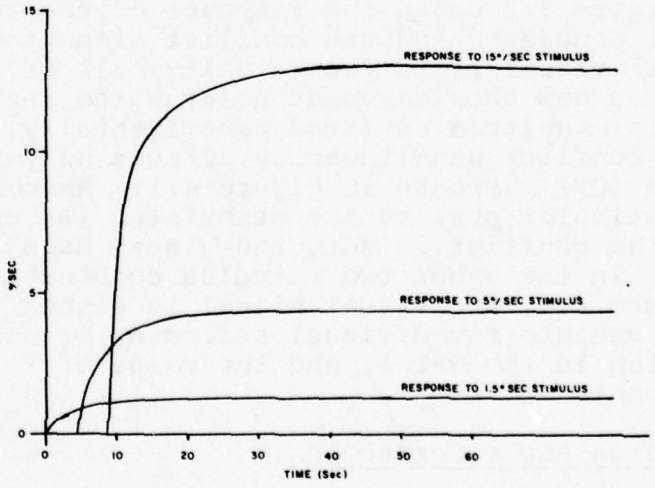

Figure 5.2 Circularvection step response of model with cue conflict element included. Stimuli are 1.5°/sec, 5°/sec, and 15°/sec steps in visual field yaw velocity beginning at t=0.

however, by using the filter g_z estimate to adjust pitch and roll angles.

5.3 Saccule Non-Linearity

Certain illusory effects associated with static orientation in different specific force environments have long been recognized and classified as Aubert, Müller, and Elevator Illusion Effects. The Aubert effect describes a typical underestimation of tilt angle in a 1g or less than 1g environment; the Müller effect refers to a characteristic overestimation of tilt angle in a greater than 1g environment; and Elevator illusion is a pitch-up sensation that often accompanies increased g_z. A more detailed description of these effects can be found in Ormsby (1974). Ormsby (1974) has shown that these effects can be generated by assuming that the non-linear function of Figure 5.3 operates on saccular otolith information, and the saccule non-linearity has, therefore, been included in the computer model as shown in Figure 5.4. Since it is in the otolith afferent pathway at the "junction" between the otolith model and the central processor model, it may be considered to be part of either.

As the model is exercised more thoroughly and as more experimental data become available, it may be necessary to further increase the complexity of the central processor model in order to obtain a more precise match with certain observed human responses. Our philosophy, however, is to retain the optimal estimator concept to the greatest degree possible.

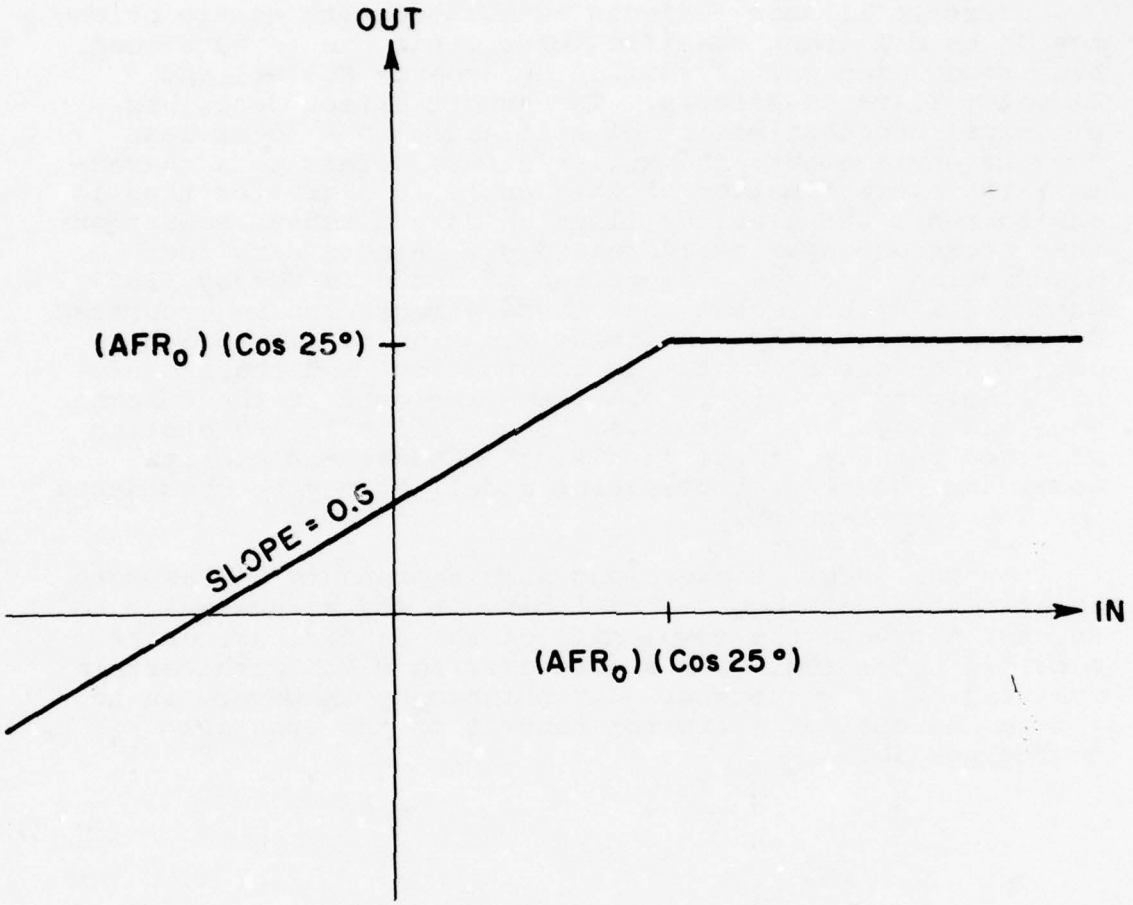

$$AFR_0 \equiv \frac{\text{AFFERENT FIRING RATE}}{g}$$

Figure 5.3 Saccule Non-linearity (redrawn from Ormsby, 1974)

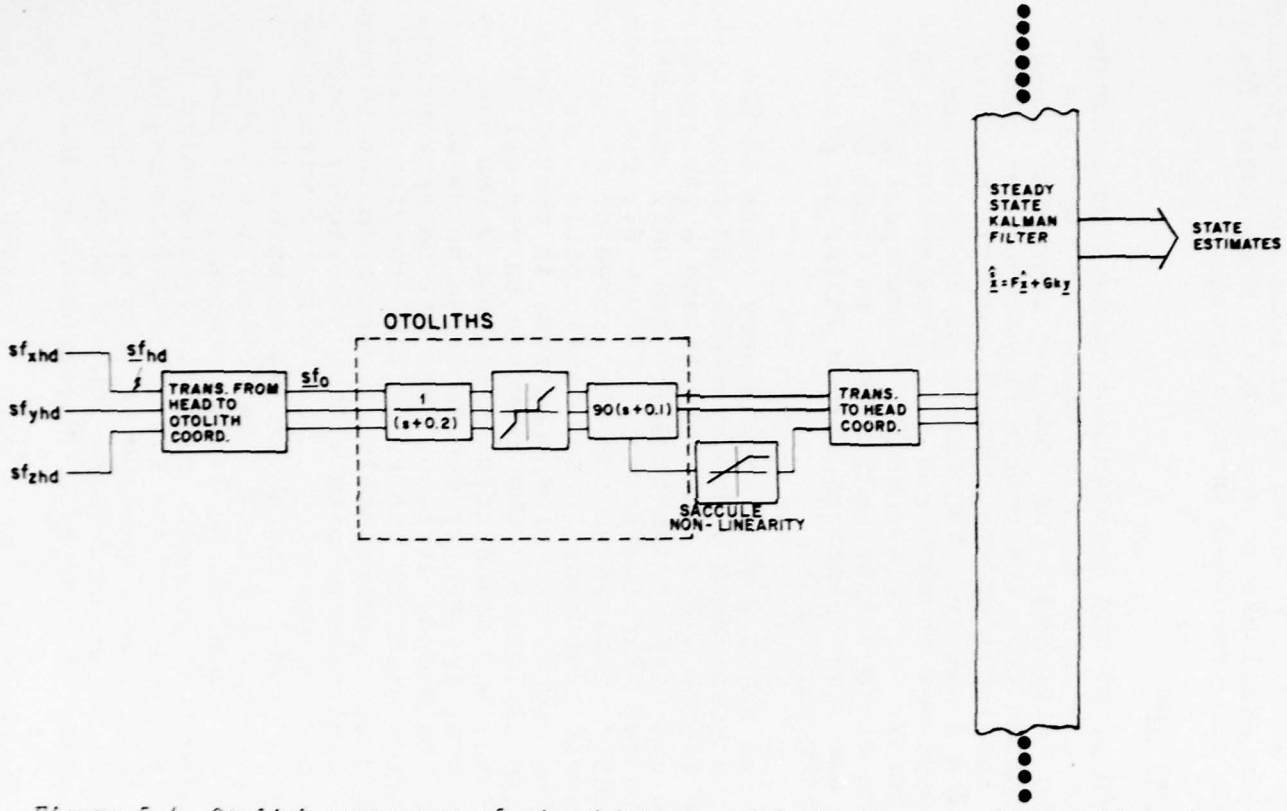

Figure 5.4 Otolith component of time history model showing saccule non-linearity.

6.0 ACTIVE PILOT

Perception is dramatically affected by mental set, and prior knowledge or expectancy of motion will certainly influence motion perception. If the multi-sensory model is to represent an active pilot as opposed to a passive naive subject, it must be extended to consider the predictive information available to the pilot. Some ideas for such extension are presented in this section.

6.1 Input Spectrum

A skilled pilot may be presumed to have an accurate expectation of the input spectrum associated with the maneuver being initiated. One modeling approach, therefore, is to assume that the central processor has correct knowledge of the input spectrum for a specific maneuver or portion of a maneuver. The Kalman gains to be used during this maneuver segment can be calculated using that specific spectrum. Since a changing input spectrum does contradict the steady-state assumption, it might be necessary to use a time-varying Kalman filter in place of the steady-state verison.

Figures 6.1 and 6.2 show preliminary tests of the above technique using both a steady-state and time-varying filter. (See figure 6.3). The stimuli are a yaw acceleration impulse and step, respectively, with only vestibular sensors considered ("in the dark"). Figure 6.1 can, therefore, be directly compared to the "RD" curve of Figure 4.1. Since the central processor is now "anticipating" or "expecting" the proper stimulus spectrum, it should make fairly accurate estimates. The response curves all have the proper slope, but orientation angle estimates have a large initial bias apparently due to large gains which may be correct in the steady-state but may not be appropriate immediately after stimulus onset. A time-varying filter should adjust gains appropriately at each sampling interval and, in fact, preliminary tests with a non-steady state approach have been encouraging. When a filter with time-varying gains is used in the above two examples (see Appendix D for specific filter formulation) the initial biases described above are no longer present, and the filter does make more accurate estimates, especially in position (see Figures 6.1b and 6.2c). Furthermore, when the internal model input spectrum is this accurate, the time-varying filter is extremely "robust" showing very little sensitivity to changes in measurement noise.

It must be recognized that even an active and experienced pilot probably does not experience sensations as accurate as these filter responses, and to be more

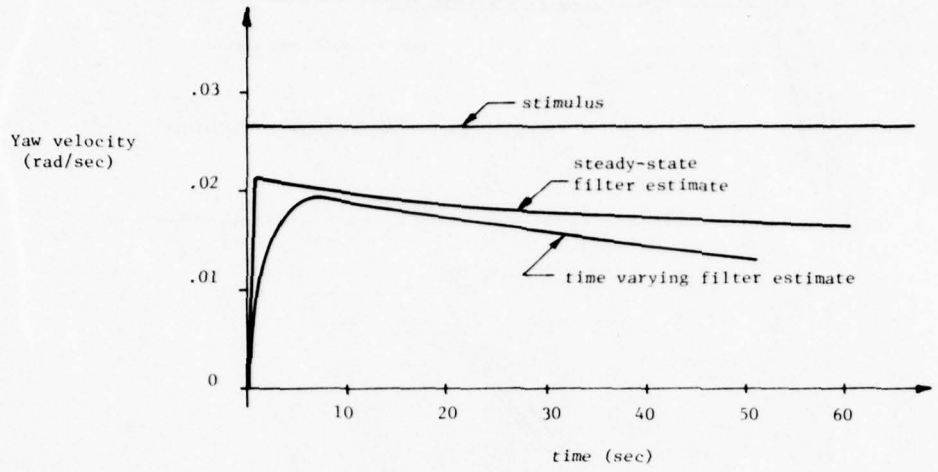

a. velocity response

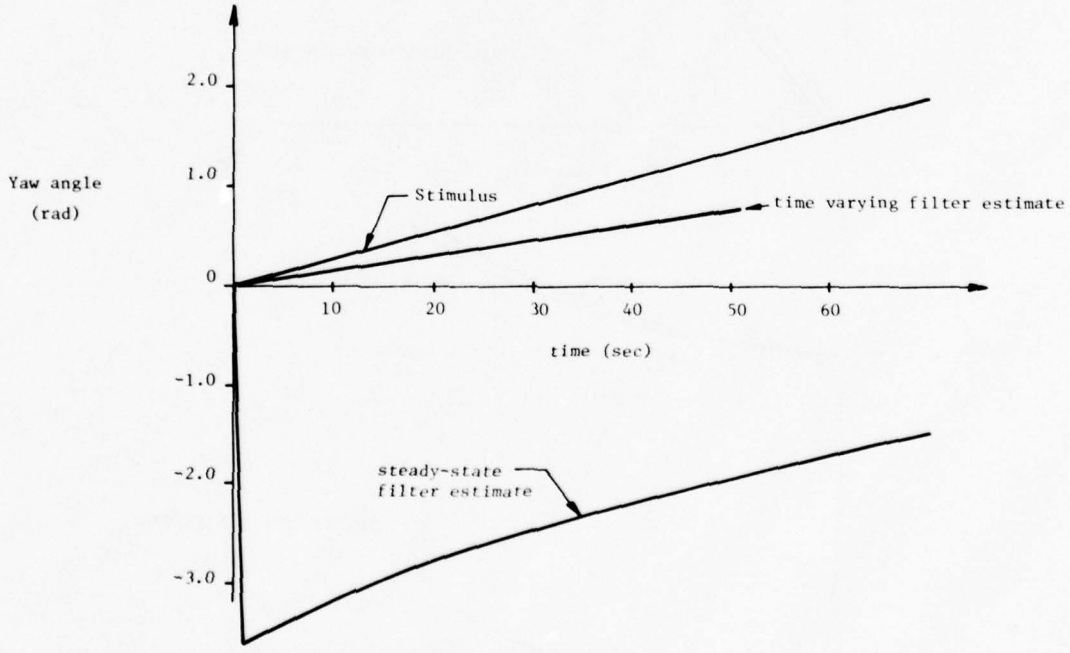

b. position response

Figure 6.1 Model response to yaw acceleration impulse (velocity step) in the dark, using Internal Model with wide band angular acceleration input approximating that of a random impulse

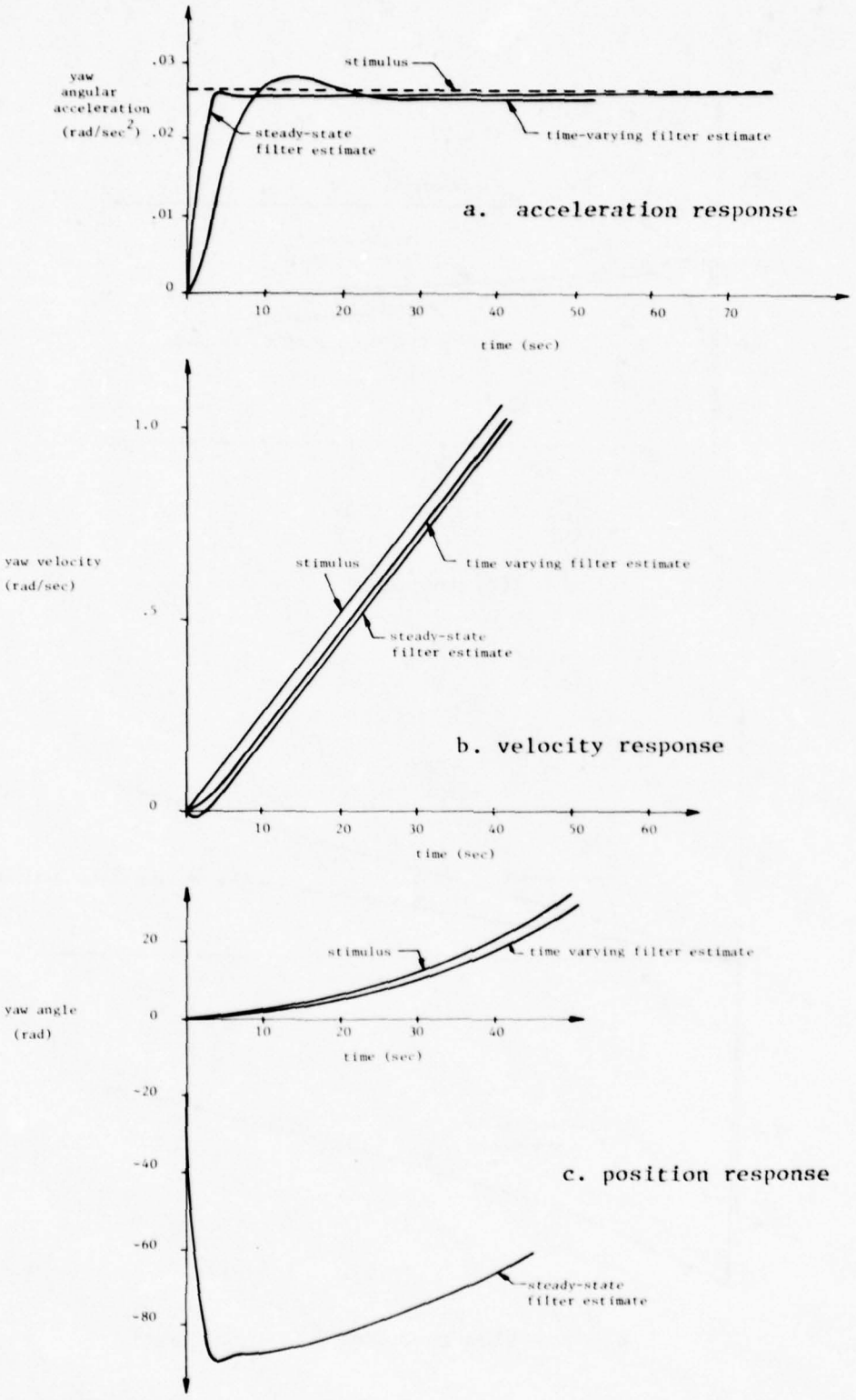

Figure 6.2 Model response to yaw angular acceleration step (velocity ramp), in the dark, using internal model with angular acceleration spectrum approximating that of a step (1/s).

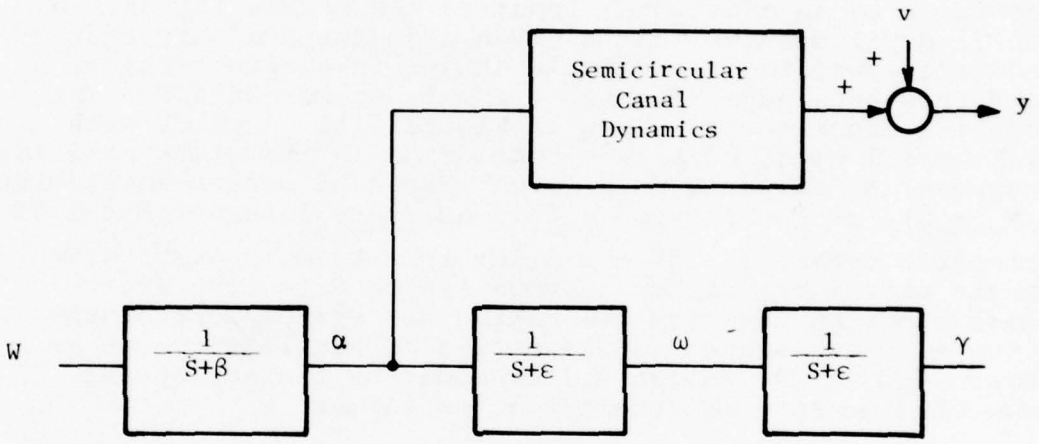

Step in α: β=.001, ε=.001

Impulse in α: β=1000., ε=.001

Figure 6.3 Internal model used to derive both steady-state and time-varying Kalman filters in figures 6.1 and 6.2. For the acceleration impulse responses of figure 6.1, β=1000, approximating a wide band random impulse spectrum. For the acceleration step responses of figure 6.2, β=.001 to approximate the spectrum of a step. Integration is approximated by first order filters with long time constants ($1/\varepsilon$).

realistic it is probably necessary to assume a less accurate expectation of stimulus spectrum. Implementation of a time-varying filter, as specified in Appendix D, is well known and certainly feasible, but more cumbersome than the steady-state version in terms of programming complexity and computer time requirements.

6.2 Control Stick Position

A second approach is to incorporate control stick position as an additional input to the Kalman filter. A skilled pilot knows that a given adjustment of aircraft controls results in a certain change in aircraft state, and thus knowledge of control input becomes data for the central processor as shown in Figure 6.4. A pilot with less skill might have less confidence in the stick position measure as reflected in a larger expected measurement noise (v_{stick}), or may rely on a less accurate internal model of aircraft dynamics. If the pilot is extremely busy, side tasks presumably siphon nervous system attention from sensor motion cue signals, making the system less sensitive to these signals. The decreased sensitivity can be expressed in the Kalman filter model by increasing the expected sensory measurement noise values.

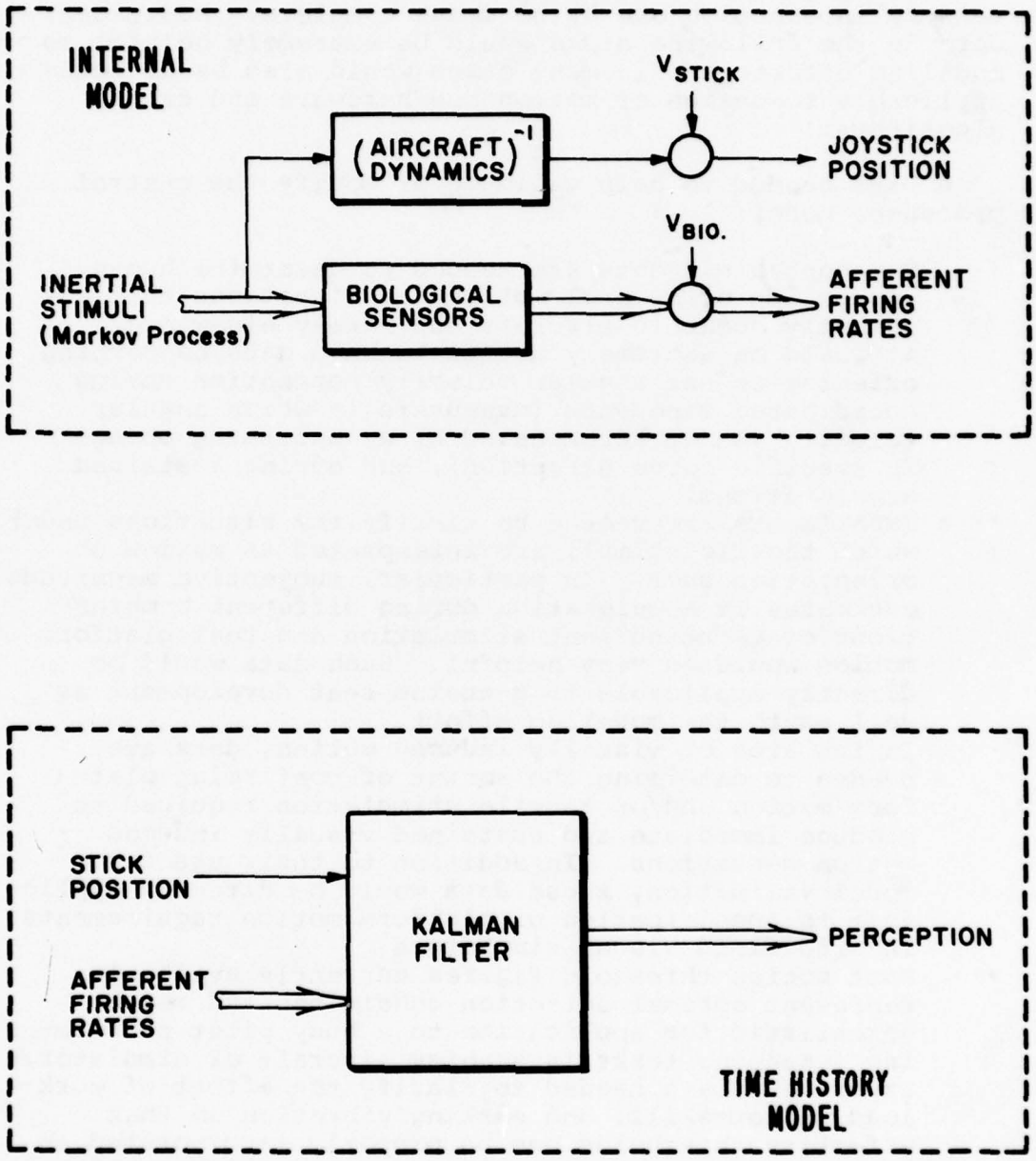

Figure 6.4 Model Extension to include Active Pilot

7.0 EXPERIMENTAL PROGRAM

The required data concerning receptor physiology and sensory interaction are by no means complete. Additional data in the following areas would be extremely helpful to modeling efforts and in many cases would also be directly applicable to design of motion cue hardware and drive algorithms.

- Data needed to help validate or modify the central processor model:

··· Psychophysical data are needed to determine human perception of several motion cue situations that commonly occur in aircraft but rarely elsewhere. It would be extremely useful to have data concerning orientation and angular velocity perception during coordinated maneuvers (maneuvers in which angular velocity is not accompanied by a confirming change in specific force direction), and during sustained accelerations.

··· Experiments are needed to clarify the situations under which tactile stimuli are interpreted as motion or orientation cues. In particular, subjective magnitude estimates of acceleration during different combinations of g-cueing seat stimulation and real platform motion would be very helpful. Such data would be directly applicable to g-cueing seat development as well as to the modeling effort.

··· In the area of visually induced motion, data are needed to determine the amount of confirming platform motion and/or tactile stimulation required to produce immediate and sustained visually induced motion sensations. In addition to their use for model validation, these data would be directly applicable to specification of platform motion requirements in wide field visual simulators.

··· Most motion threshold figures currently available represent optimal detection conditions and may be unrealistic for application to a busy pilot performing demanding tasks in a noisy aircraft or simulator. Experiments are needed to clarify the effect of workload, pilot skill, and masking vibration so that effective thresholds can be properly incorporated in perception models and applied to simulation problems.

- Data needed to validate or modify individual sensor models:

··· There are currently very few data available to support the head-neck proprioception model described in this report. Measurements of dynamic head displacement under lateral and longitudinal gravito-inertial force, as well as electro-physiological measurements of head-neck system response during such stimuli would be a great aid.

··· The tactile cue processing model currently employed is based primarily on data generated from neural recordings or vibro-tactile threshold measures in which small area stimuli were applied to the forearm or hand. Threshold and sensitivity to broad area tactile stimulation over the back and buttocks need to be investigated so that the tactile model component can be improved and expanded.

- Data to determine the proper stimulus input to the model:

··· The relation between aircraft motion and body-seat pressure currently is not well known, yet is very important to the modeling effort since it forms the input to the tactile component of the multi-sensory model. Studies of dynamic body-seat pressure distribution in response to changes in gravito-inertial force, especially during typical aircraft maneuvers, will be a great aid both in modeling and in development of g-cueing seat drive algorithms.

Several specific experiments have been proposed to address some of the needs listed above and are described in the following sections. Preparations are currently underway for two of these experiments (flight experiment and minimum platform motion experiment) and a third (vibration masking effect experiment) is in progress.

7.1 Flight Experiment to Study Motion Perception and Motion Cue Environment

It has been proposed that the Air Force Total In-Flight Simulation (TIFS) be used to gather psychophysical motion perception data and to simultaneously study several aspects of the motion cue environment during standardized maneuvers. The maneuvers, which include coordinated turns, "roller coaster motions," and sustained longitudinal accelerations, are designed to emphasize stimuli which cannot be adequately represented in existing motion-based simulators. Measurements will be made of perceived direction of vertical and magnitude estimates of roll rate and

translatory acceleration using a special indicator and employing an otherwise passive subject. The dynamics of seat pan and backrest pressure distribution for both the pilot and passive subject will be measured with a set of pressure transducers sewn into or laid over the seats. Video tape recordings of the pilot's and passive subject's head positions with respect to the cockpit will be made for later analysis and neck muscle activity will also be measured using EMG electrodes. Full documentation of the aircraft's specific forces, angular rates and Euler angles will be obtained from an on-board inertial system.

The subjective spatial orientation and subjective angular velocity results will be used for validating or improving response of the model's central processor. Head motion and head EMG data will be useful for validating the head-neck proprioception model component since one state of this model corresponds to head position and another to neck muscle activity, and will also be used to study the difference between the passive subject and active pilot response. In addition, this part of the experiment may provide some of the data base needed for development of g-cueing devices that apply force to the head-neck system. Body-seat force measurements will be used to determine proper input to the tactile model, to serve as a partial data base for development of g-cueing seat algorithms, and to study the differences between active pilots and passively moved subjects by noticing differences in tactile stimuli due to anticipatory body tensing, etc.

7.2 Vibration Masking Effect Experiment

The NASA Man Carrying Rotation Device (MCRD), because of its capacity for smooth rotation, is ideally suited for study of yaw acceleration threshold and time-to-detect as a function of masking vibration frequency and amplitude. Such an experiment has been planned with Mr. John Stewart and implemented at NASA-Ames Research Center. Complete experimental plans called for four to six different acceleration levels combined with masking vibration at two different amplitudes and with four different frequency spectra. A peak threshold level of .3 to .5 degrees/sec^2 and an above threshold level of 1-2 degrees/sec^2 were the planned vibration amplitudes. The frequency spectra were tentatively chosen as 5, 2 and .6 Hz sine waves as well as one pseudo-random signal with frequency content in the 5 to .6 Hz range. An initial simplified protocol has been run at Ames Research Center. Although the experiment is still in progress, preliminary results indicate that thresholds may be affected by pseudo-random signal vibrations but might not be affected by pure sinusoidal vibration.

Results from this experiment will be used to help set realistic threshold values in the multi-sensory model and may be directly applicable to design of simulator "washout" algorithms; for instance, if threshold can be raised briefly by superimposed aircraft noise, this might permit the system to be driven closer to its limits employing more abrupt washout decelerations.

7.3 Minimum Platform Motion Experiment

The following experiment is suggested for implementation on a moving-based simulator with wide field visual display capability:

- Using one motion axis at a time (for instance, yaw motion) apply a truncated ramp in visual field velocity.
- Apply platform acceleration doublets of varying magnitude in conjunction with the visual stimuli as shown in Figure 7.1.
- Ask subjects to control the needle position of a calibrated meter to continually estimate their perceived velocity relative to some standard or modulus.
- Before each successive trial, adjust the magnitude of the platform acceleration doublet, according to a double staircase algorithm, to find the minimum platform displacement for immediate and sustained vection. "Immediate" may be defined as the time to respond to completely confirming platform and visual motions of equal magnitude. "Sustained" may be defined as a deviation of less than $\pm\Delta$ from the "immediate" response.
- Repeat the experiment with g-cueing seat stimulation added.

Dr. David Quam, University of Dayton, is currently incorporating a similar protocol in an experimental program on the Air Force Flight Dynamics Laboratory, Large Amplitude Multi-Mode Aerospace Research System (LAMARS) on Air Force Contract F33615-77-C-0080. Stimuli used in the experiment will subsequently be used to drive the multi-sensory model, and model central processor responses can thus be compared to experimental magnitude estimation data. Results from the experiment may also be directly applied to determination of simulator platform motion requirements.

7.4 G-Cueing Seat Experiment

The g-cueing seat permits variation of body-seat pressure distribution and is therefore an ideal tool for studying the way in which tactile stimuli are interpreted

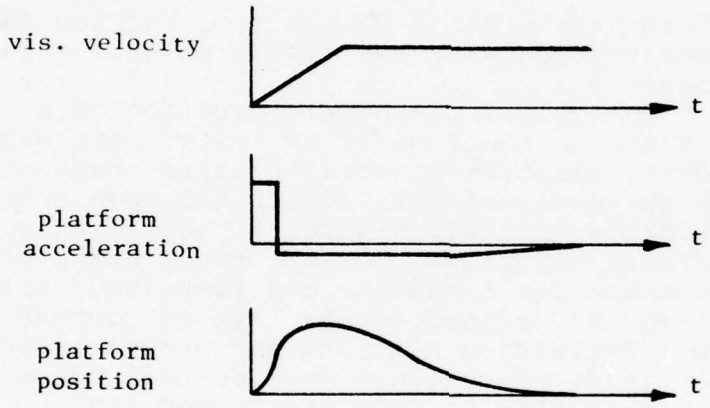

Figure 7.1 Visual field motion with platform motion onset cue.

as motion cues. The following experiment is suggested to create a preliminary data base in this area:

- Use the body-seat pressure sensing device, previously suggested for use in the flight experiment, to measure dynamic pressure distribution created by g-seat stimuli with and without platform motion.
- Adjust g-seat drive logic to obtain the best match with data from the previously described flight experiment.
- Simulate a sustained, translatory acceleration on a moving base simulator using base motion alone, g-seat cueing alone, and combined base and g-seat cueing.
- During some runs, ask subjects to continuously track perceived earth vertical using an instrumented pointer device.
- During other runs, ask subjects to continuously estimate acceleration (or velocity) magnitude, as compared to some reference or standard, by controlling the needle of a zero centered meter.

Since perception is heavily influenced by mental set, the subject must be in an environment where motion is believed to be possible. Therefore, it is important that platform motion alone, g-seat cueing alone, and combined g-seat and platform motions all take place on the same device and during the same experimental sessions. Results from the above experiment will be useful as a data base for validation of tactile-vestibular cue blending by the multi-sensory model central processor, and in addition, the results may provide some insights into optimal design of g-cueing seat drive algorithms.

7.5 Characteristics of Vibro-Tactile Sensation on the Back and Buttocks

The following experiment is suggested to provide a data base for tactile sensor system modeling:

- Construct a seat with a portion of the seat pan and seat back "cut-out"
- Construct a controlled force vibrator, with interchangeable contactors of varying surface area, to operate through the cut-out portions of the seat.
- Find the subjective threshold to tactile stimuli as a function of frequency, contactor surface area, and body placement of the contactor. This can be accomplished by varying one parameter at a time and using the double staircase technique to approach the threshold from above and below.

- Use a subjective magnitude estimation technique to determine sensation intensity as a function of frequency, contactor surface area, and placement of contactor.

8.0 CONCLUSION

A multi-sensory motion perception model has been developed using an optimal estimation approach to the integration of multiple sensory inputs. Although the biological system is far more complex than the linear estimator used in the model, the linear estimator alone has proven capable of exhibiting correct, qualitative human response characteristics to a surprising degree. Some highly non-linear characteristics such, as the well-documented delay in onset of visually induced motion, are not produced by the linear central processor but can be generated by adding non-linear elements to the central processor model.

It is felt that additional improvement and extension of the multi-sensory model is possible with further development work, including representation of the active pilot; however, additional experimental data in certain areas are badly needed to support such effort. In its eventual application, the model will be useful in objectively predicting motion cue requirements for ground simulation, and developing drive algorithms to produce the highest simulator fidelity under given hardware limitations.

9.0 REFERENCES

1. Berthoz, A., Pavard, B., & Young, L.R. Perception of Linear Horizontal Self-Motion Induced by Peripheral Vision (Linearvection): Basic Characteristics and Visual-Vestibular Interactions. Exp. Brain Research, 23:471-489, (1975).

2. Borah, J., Young, L.R., & Curry, R.E. Sensory Mechanism Modeling, Interim Report. AFHRL-TR-77-70, AD-A049 278. Wright-Patterson AFB, Ohio: Advanced Systems Division, Air Force Human Resources Laboratory, October 1977.

3. Borah, J. Human Dynamic Orientation Model Applied to Motion Simulation. S.M. Thesis, Department of Aeronautics and Astronautics, MIT, (1976).

4. Brandt, Th., Wist, E.R. & Dichgans, J.M. Foreground and Background in Dynamic Spatial Orientation. Perception and Psychophysics, 17:497-503, (1975).

5. Brandt, T., Dichgans, J., & Koenig, E. Differential Effects of Central Versus Peripheral Vision of Egocentric and Exocentric Motor Perception. Experimental Brain Research, 16:476-491, (1973).

6. Chambers, M.R., Andres, K.H., Duering, M., & Iggo, A. The Structure and Function of the Slowly Adapting Type II Mechanoreceptor in Hairy Skin. Quart. J. Exp. Physiol., 57:417-455, (1972).

7. Chu, W. Dynamic Response of Human Linearvection. S.M. Thesis, Department of Aeronautics and Astronautics, MIT, (1976).

8. Cohen, M.M., Crosbie, R.J. & Blackburn, L.H. Disorienting Effects of Aircraft Catapult Launchings. Aerospace Med., 44(1):37-39, (1973).

9. Fernandez, C. & Goldberg, J.M. Physiology of Peripheral Neurons Innervating Otolith Organs of the Squirrel Monkey, I, II, and III. J. Neurophysiol., 39:970-1008, (1976).

10. Gelb, A., VanderVelde, W.E. Multiple Input Describing Functions and Nonlinear System Design, New York, McGraw-Hill, (1968).

11. Goldberg, J.M. & Fernandez, C. Physiology of Peripheral Neurons Innervating Semicircular Canals of the Squirrel Monkey, I, II, and III. J. Neurophysiol., 34:661-675, (1971).

12. Graybiel, A. & Brown, R.H. The Delay in Visual Reorientation Following Exposure to a Change in Direction of Resultant Force on a Human Centrifuge. J. Gen. Psychol., 45, (1951).

13. Gum, D.R. Modeling of the Human Force and Motion-Sensing Mechanisms. AFHRL-TR-72-54, AD-766 444. Wright-Patterson AFB, Ohio: Advanced Systems Division, Air Force Human Resources Laboratory, June (1973).

14. Held, R., Dichgans, J.M. & Bauer, J. Characteristics of Moving Visual Scenes Influencing Spatial Orientation. Vision Research, 14:1-9, (1974).

15. Iggo, A. & Muir, A.R. The Structure and Functions of a Slowly Adapting Touch Corpuscle in Hairy Skin. J. Physiol., 300:762-769, (1969).

16. Lichtenstein, J.H. & Saucer, R.T. Experimental Investigation of the Visual Field Dependency in the Erect and Supine Positions. NASA TN D-6883, (1972).

17. Lowenstein, W.R. Mechano-electric Transduction in the Pacinian Corpuscle. Handbook of Sensory Physiology, Vol. I, W.R. Lowenstein (Ed.), Springer-Verlag, Berlin, (1971).

18. Ormsby, C. Model of Human Dynamic Orientation. Ph.D. Thesis, Department of Aeronautics and Astronautics, MIT, (1974).

19. Sandell, N.R. & Athans, M. Modern Control Theory -- Computer Manual, Center for Advanced Engineering Study, Massachusetts Institute of Technology, Cambridge, (1974).

20. Wolfe, J.W. & Cramer, R.L. Illusions of Pitch Induced by Centripetal Acceleration. Aerospace Med., 41(10): 1136-1139, (1970).

21. Young, L.R. Role of the Vestibular System in Posture and Movement. In: Medical Physiology, V.B. Mountcastle (Ed.) 13th Edition, Volume I, Chapter 27, St. Louis: C.V. Mosby and Company, (1974).

22. Young, L.R. & Meiry, J.C. A Revised Dynamic Otolith Model. Aerospace Med., 39(6):606-608, (1968).

23. Young, L.R. & Oman, C.M. Model for Vestibular Adaptation to Horizontal Rotation. Aerospace Med., 40: 1076-1080, (1969).

24. Zacharias, G.L. & Young, L.R. Manual Control of Yaw Motion With Combined Visual and Vestibular Cues. Annual Conference on Manual Control, MIT, (1977).

APPENDIX A

STEADY-STATE KALMAN FILTER GAIN CALCULATION

The entire internal model of Figure 3.2 can be expressed in state vector form as:

$$\dot{\underline{x}} = A\,\underline{x} + E\,\underline{w}$$
$$\underline{y} = C\,\underline{x} + \underline{v} \qquad \text{(A.1)}$$

where

$$\underline{x} = \begin{bmatrix} \underline{vel} \\ \underline{acc} \\ \underline{\gamma} \\ \underline{\omega} \\ \cdot \\ \cdot \\ \cdot \\ \cdot \\ x_{nx} \end{bmatrix} \equiv \text{State vector of dimension nx}$$

$A \equiv$ system matrix of dimension nx by nx

$E \equiv$ input matrix of dimension nx by nw

$\underline{y} \equiv$ output vector (representing afferent signals) of dimension ny

$C \equiv$ output observation matrix of dimension ny by nx

$\underline{W} \equiv$ white process noise vector of dimension nw

$\underline{v} \equiv$ white measurement noise vector of dimension ny

$nx \equiv$ number of state variables

$nw \equiv$ number of white noise inputs

number of output observations

Note that $\underline{\gamma}$, $\underline{\omega}$, $\underline{vel}$, and $\underline{acc}$ (see Figure 3.2) must appear as state variables since the estimates of these states will represent the perceptual quantities desired. The remaining state variables need not have any physical significance.

Optimal steady-state Kalman filter gains are determined from the model of Equation A.1 by solving the following matrix equations.

1. Covariance of state (X).

   X is the solution of the linear matrix equation.

$$\dot{X} = 0 = A\,X + X\,A' + E\,Q\,E' \qquad (A.2)$$

   where $Q \equiv$ power spectral density of $\underline{W}$

2. Covariance of observation (Y).

$$Y = C\,X\,C' \qquad (A.3)$$

3. Power spectral density of measurement noise (R)

$$R_{ij} = 0 \quad (i \neq j)$$
$$R_{ii} = \rho_i\, Y_{ii} \qquad (A.4)$$

4. Error Covariance of the Kalman filter (P).

   P is the solution of the Matrix Riccati equation.

$$\dot{P} = 0 = A\,P + P\,A' + E\,Q\,E' - P\,C'\,R^{-1}\,C\,P \qquad (A.5)$$

5. Covariance of the Kalman filter estimate (XH).

$$XH = X - P \qquad (A.6)$$

6. Steady-state Kalman filter gain matrix (GK)

$$GK = P\,C'\,R^{-1} \qquad (A.7)$$

7. Filter system matrix (F)

$$F = (A - GK\,C) \qquad (A.8)$$

Note that the "ratio", ρ, in equation A.4, relates noise power spectral density to signal variance and, therefore, has units of seconds.

A.1 Linear Matrix Equation Solution

The linear matrix equation is solved using a FORTRAN IV subroutine listed in Sandell and Athans (1974). The equation:

$$0 = G' X + X G + C1 \tag{A.9}$$

where $G = A'$

is solved numerically by computing the series

$$X_k = (F')^{2^{k-1}} X_{k-1} F^{2^{k-1}} + X_{k-1};\ k=1,2,... \tag{A.10}$$

where $F = 2 (t G - I)^{-1} + I$

$X_o = 2t (t G' - I)^{-1} C1 (t G - I)^{-1}$

$t = \min \{1, -4n/\text{trace}(g)\}$

The convergence test is

$$(X_k)_{ii} - (X_{k-1})_{ii} \leq TOL * (X_k)_{ii} \tag{A.11}$$

A.2 Riccati Equation Solution

The Ricatti equation is also solved with a subroutine from Sandell and Athans (1974).

$$0 = G' P + P G + C1 + P C2 P \qquad (A.12)$$

where $G = A'$

is solved by repeatedly solving the linear equation

$$0 = (G - C2\ P_{n-1})'\ P_n + P_n\ (G - C2\ P_{n-1}) + C3 \qquad (A.13)$$

where $C3 = C1 + P_{n-1}\ C2\ P_{n-1}$

P_o is chosen to numerically solve

$$P_o = \{\int_o^T e^{-Gt}\ C2\ e^{-G't}\ dt\}^{-1} \qquad (A.14)$$

APPENDIX B

TIME RESPONSE CALCULATION

Once the optimal Kalman gains have been calculated the filter can be implemented by satisfying

$$\dot{\hat{\underline{x}}} = F\,\hat{\underline{x}} + Gk\,\underline{y} \qquad \text{(B.1)}$$

y_i are afferent signals received by the filter and x_i are the filter's estimates of internal model states.

The linear portion of each sensor model can be represented in state variable form as

$$\begin{aligned} \dot{\underline{x}} &= A\,\underline{x} + B\,\underline{u} \\ \underline{y} &= C\,\underline{x} \end{aligned} \qquad \text{(B.2)}$$

where $\underline{x}$ = sensor state vector
B = sensor input matrix
$\underline{u}$ = deterministic stimulus
$\underline{y}$ = afferent response
C = sensor output matrix

Equation B.2 can be implemented on a computer by the discrete formulation

$$\underline{x}(t) = \Phi(\Delta t)\,\underline{x}(t-\Delta t) + DM(\Delta t)\,\underline{u}(t) \qquad \text{(B.3)}$$

$$\Phi(\Delta t) = e^{A\,\Delta t} \qquad \text{(B.4)}*$$

$$DM = \{\int_0^{\Delta t} \Phi(\nu)\,d\nu\}B \qquad \text{(B.5)}$$

---

* For a square matrix A, the matrix exponential is defined as:

$$e^A = I + A + \frac{A^2}{2!} + \frac{A^3}{3!} + \ldots$$

This formulation assumes that u(t) is approximated by a series of ΔT duration steps.

The filter (equation B.1) is implemented on the computer in a similar fashion by the relation

$$\underline{x}(t) = \Phi_F(\Delta t)\ \underline{x}(t-\Delta t) + DM_F(\Delta t)\ \underline{y}(t) \qquad (B.6)$$

$$\Phi_F = e^{F\ \Delta t} \qquad (B.7)$$

$$DM_F = \{\int_0^{\Delta t} \Phi_F(\nu)\ d\nu\}\ GK \qquad (B.8)$$

APPENDIX C

INTERNAL MODEL PARAMETERS AND EXAMPLE OF STEADY-STATE KALMAN FILTER CONSTRUCTION

C.1 Internal Model Parameters Used to Generate Time Responses In Section 4.0

(Refer to Figures 3.2, 3.3 and 3.4)

The elements of the vectors shown below correspond to xhd, yhd, and zhd axes (see Figure 3.1). The input noise power-density spectrum (Q) is actually a square matrix whose off-diagonal elements (cross-power spectral densities) are zero. Only the non-zero, diagonal elements are given below, in vector form. The tactile sensor noise ratio ($\underline{\rho}_t$) is shown with only two elements (corresponding to xhd and zhd axes), since the model currently considers only one tactile signal from the seat-pan and one from the backrest. The current proprioceptive model considers only lateral head-neck motion, and $\underline{\rho}_p$, therefore, has only a yhd component.

INPUT PROCESS, WHITE NOISE POWER SPECTRAL DENSITY

$$Q_{rot} = \begin{bmatrix} 3 \times 10^4 \\ 3 \times 10^4 \\ 3 \times 10^4 \end{bmatrix} \equiv \text{power spectral density of } \underline{W}_{rot}$$

$$Q_{tran} = \begin{bmatrix} 0.5 \\ 0.5 \\ 0.5 \end{bmatrix} \equiv \text{power spectral density of } \underline{W}_{tran}$$

INPUT PROCESS BANDWIDTH

$$\underline{\beta}_{rot} = \begin{bmatrix} 120 \\ 120 \\ 200 \end{bmatrix}$$

$$\underline{\beta}_{tran} = \begin{bmatrix} 2.0 \\ 2.0 \\ 2.0 \end{bmatrix}$$

MEASUREMENT NOISE RATIOS

(Noise Power Spectral Density)/(Signal Variance)

$$\underline{\rho}_c = \begin{bmatrix} .0005 \\ .0005 \\ .001 \end{bmatrix}$$

$$\underline{\rho}_o = \begin{bmatrix} .001 \\ .001 \\ .001 \end{bmatrix}$$

$$\underline{\rho}_{\text{vis. rot.}} = \begin{bmatrix} .01 \\ .01 \\ .003 \end{bmatrix} \quad \underline{\rho}_{\text{vis. tran.}} = \begin{bmatrix} .01 \\ .01 \\ .01 \end{bmatrix} \quad \underline{\rho}_{\text{vis. hor.}} = \begin{bmatrix} .01 \\ .01 \\ .01 \end{bmatrix}$$

$$\underline{\rho}_t = \begin{bmatrix} .001 \\ .001 \end{bmatrix}$$

$$\underline{\rho}_p = .001$$

C.2 Example: Construction of Filter Used to Model Visual-Vestibular Interaction During Yaw Motion

For the following example, the yaw channel has been decoupled from the diagram of Figure 3.2 (as described in section 3.4), and the resulting internal model is shown in Figure C.1 Semicircular canal dynamics and input process dynamics have been expanded to show all of the state variables, but are equivalent to the transfer functions in Figure 3.2. The A, C, and E matricies used below are determined directly from the diagram of Figure C.1. Q_{rot}, ρ_c, and $\rho_{\text{vis. rot.}}$ are the zhd axis values (third elements of the respective vectors) listed in section C.1.

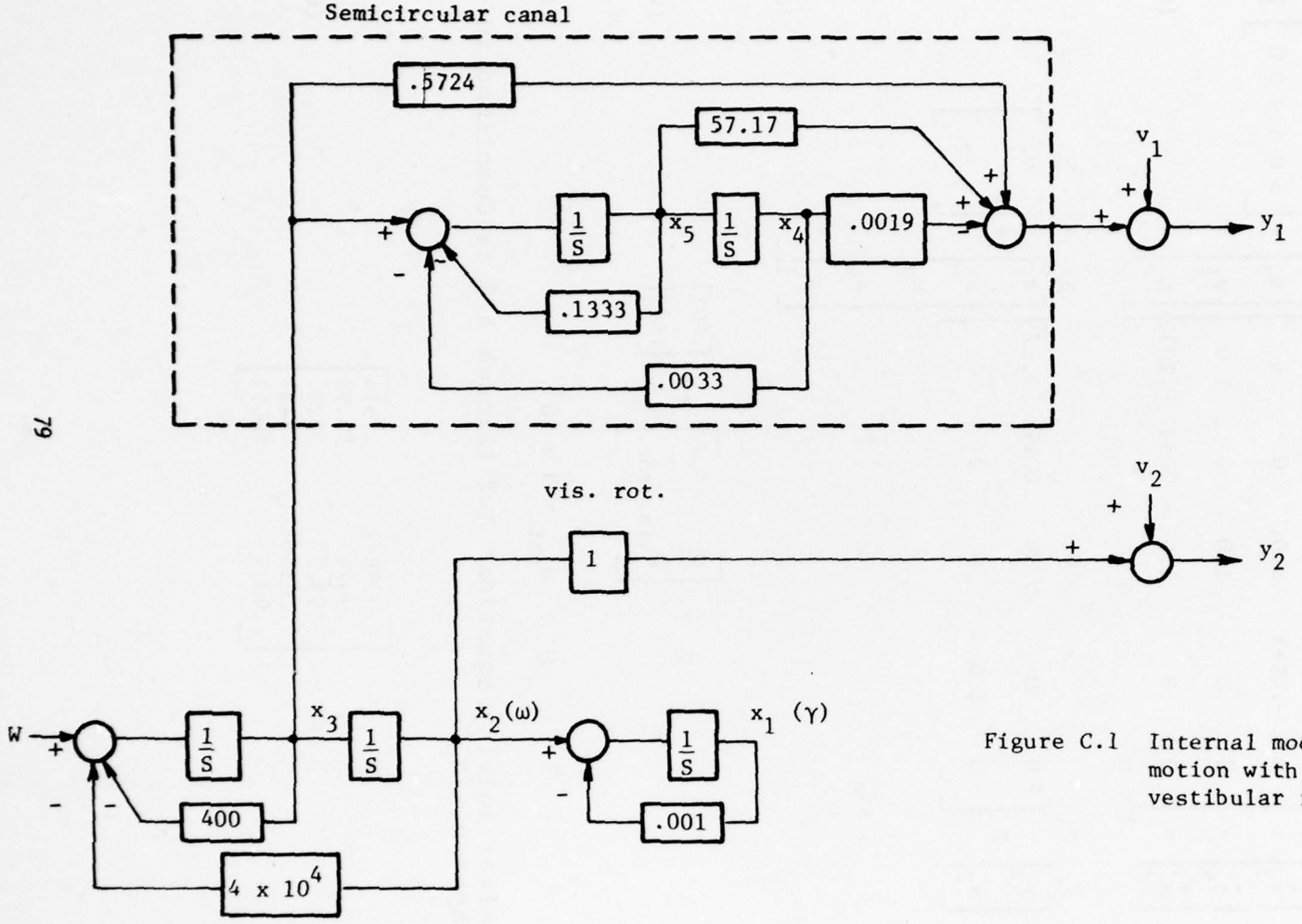

Figure C.1 Internal model for yaw motion with visual-vestibular interaction

$$\dot{\underline{x}} = A\,\underline{x} + E\,\underline{W}$$

$$\begin{bmatrix} \dot{x}_1 \\ \dot{x}_2 \\ \dot{x}_3 \\ \dot{x}_4 \\ \dot{x}_5 \end{bmatrix} = \begin{bmatrix} -.001 & 1.0 & 0 & 0 & 0 \\ 0 & 0 & 1.0 & 0 & 0 \\ 0 & -.4E+5 & -400. & 0 & 0 \\ 0 & 0 & 1.0 & 0 & 1.0 \\ 0 & 0 & 1.0 & -.0033 & -.1333 \end{bmatrix} \begin{bmatrix} x_1 \\ x_2 \\ x_3 \\ x_4 \\ x_5 \end{bmatrix} + \begin{bmatrix} 0 & 0 & 1.0 & 0 & 0 \end{bmatrix} \underline{W} \qquad \text{(C.1)}$$

$$\underline{y} = C\,\underline{x} + \underline{v}$$

$$\begin{bmatrix} y_1 \\ y_2 \end{bmatrix} = \begin{bmatrix} 0 & 0 & .5724 & .0019 & 57.17 \\ 0 & 1.0 & 0 & 0 & 0 \end{bmatrix} \begin{bmatrix} x_1 \\ x_2 \\ x_3 \\ x_4 \\ x_5 \end{bmatrix} + \begin{bmatrix} v_1 \\ v_2 \end{bmatrix} \qquad \text{(C.2)}$$

$$\underline{\rho} = \begin{bmatrix} \rho_c \\ \rho_{vis.\ rot.} \end{bmatrix} = \begin{bmatrix} .001 \\ .003 \end{bmatrix} \qquad \text{(C.3)}$$

$$\underline{Q} = Q_{rot} = 3 \times 10^4 \qquad \text{(C.4)}$$

After solving equations A.2 through A.8 as described in Appendix A,

$$GK = \begin{bmatrix} -.399E-2 & .7914 \\ .9024 & 50.99 \\ 863.2 & 3523. \\ -.1638E-2 & .5451 \\ .9027 & 50.91 \end{bmatrix} \qquad \text{(C.5)}$$

$$F = \begin{bmatrix} .001 & .2086 & .2284E\text{-}2 & -.7613E\text{-}5 & .2281 \\ 0 & -50.99 & .4835 & .1722E\text{-}2 & -51.59 \\ 0 & -.4752E{+}5 & -894.1 & 1.647 & -.4935E{+}5 \\ 0 & -.5451 & .9378E\text{-}3 & -.3126E\text{-}5 & 1.094 \\ 0 & -50.91 & .4833 & -.1611E\text{-}2 & -51.74 \end{bmatrix} \quad (C.6)$$

The filter is employed in the time domain, as described in Appendix B, by satisfying

$$\dot{\hat{\underline{x}}} = F\,\hat{\underline{x}} + GK\,\underline{y}$$

$$\begin{bmatrix} \dot{\hat{x}}_1 \\ \dot{\hat{x}}_2 \\ \dot{\hat{x}}_3 \\ \dot{\hat{x}}_4 \\ \dot{\hat{x}}_5 \end{bmatrix} = \begin{bmatrix} & & \\ & F & \\ & & \end{bmatrix} \begin{bmatrix} \hat{x}_1 \\ \hat{x}_2 \\ \hat{x}_3 \\ \hat{x}_4 \\ \hat{x}_5 \end{bmatrix} + \begin{bmatrix} & & \\ & GK & \\ & & \end{bmatrix} \begin{bmatrix} y_1 \\ y_2 \end{bmatrix} \quad (C.7)$$

where $\hat{x}_i$ are the filter's estimates of internal model states (x_i), and y_1 and y_2 are time domain, yaw axis, outputs of the semicircular canal and visual field rotation models respective. (See section 2.1 for descriptions of the individual sensor models). If the visual-vestibular cue conflict non-linearity is to be used, the vision model output (y_2) is pre-processed, as described in section 5.1, before being used in equation C.7.

The digital implementation of equation C.7, as described in Appendix B, employs a transition matrix (Φ_F) and driving matrix (DM_F) which are functions of the chosen iteration interval (Δt). The values shown in equation C.8 are for an interation interval of 1 second.

$$\underline{\hat{x}}(t) = \Phi_F(1\text{sec}) \quad \hat{x}(t-1\text{sec}) + DM_F(1\text{sec}) \quad \underline{y}(t)$$

$$\begin{bmatrix} \hat{x}_1(t) \\ \hat{x}_2(t) \\ \hat{x}_3(t) \\ \hat{x}_4(t) \\ \hat{x}_5(t) \end{bmatrix} = \begin{bmatrix} .999 & .8402E\text{-}3 & .3257E\text{-}5 & -.19E\text{-}5 & .4637E\text{-}3 \\ 0 & .4570 & .1861E\text{-}6 & .1621E\text{-}2 & -.4568 \\ 0 & 1.733 & .7090E\text{-}6 & .7348E\text{-}2 & -1.733 \\ 0 & -.7647 & .2339E\text{-}5 & .9987 & .7674 \\ 0 & -.4344 & -.1769E\text{-}6 & -.1529E\text{-}2 & .4343 \end{bmatrix} \begin{bmatrix} \hat{x}_1(t\text{-}1\text{sec}) \\ \hat{x}_2(t\text{-}1\text{sec}) \\ \hat{x}_3(t\text{-}1\text{sec}) \\ \hat{x}_4(t\text{-}1\text{sec}) \\ \hat{x}_5(t\text{-}1\text{sec}) \end{bmatrix}$$

$$+ \begin{bmatrix} -.9638E\text{-}5 & .8686 \\ .9121E\text{-}2 & .3937 \\ .386E\text{-}1 & -31.77 \\ .3156E\text{-}2 & .6656 \\ .8802E\text{-}2 & .3003 \end{bmatrix} \begin{bmatrix} y_1(t) \\ y_2(t) \end{bmatrix} \qquad (C.8)$$

Although equation C.8 updates the entire state vector estimate, the elements of interest are $\hat{x}_1$ and $\hat{x}_2$ since these represent perception of angular position (γ) and angular velocity (ω) respectively.

APPENDIX D

DISCRETE, TIME-VARYING KALMAN FILTER

Given an internal model of the form

$$\dot{\underline{x}} = A\underline{x} + E\underline{w}$$
$$\underline{y} = C\underline{x} + \underline{v} \qquad \text{(D.1)}$$

where $\underline{w}$ and $\underline{v}$ are unbiased white noise processes with power spectral densities Q and R, respectively, assume that observations ($\underline{y}$) are available only at discrete times t_n, where

$$t_n = t_{n-1} + \Delta t \qquad n = 1, 2, 3, 4... \qquad \text{(D.2)}$$

If an estimate, x_{n-1}, is available for time t_{n-1}, the error covariance at time t_n, just <u>prior</u> to the measurement, can be computed as

$$P_n(-) = \Phi\ P_{n-1}(+)\ \Phi' + Q_{n-1} \qquad \text{(D.3)}$$

where $\Phi = e^{A\Delta t}$

Q_{n-1} = covariance of the process noise sequence, $\underline{w}_{n-1}$

$P_{n-1}(+)$ = error covariance at time t_{n-1}, just <u>after</u> the measurement

$P_n(-)$ can be used to calculate an optimal gain matrix

$$GK_n = P_n(-)\ C'\{C\ P_n(-)\ C' + R_n\}^{-1} \qquad \text{(D.4)}$$

where R_n = covariance of the meas. noise sequence, v_n

The optimal least-mean-squared error state estimate at time t_n is given by

$$\underline{x}_n = \Phi\ \underline{\hat{x}}_{n-1} + GK_n\ \{\underline{y}_n - C\ \Phi\ \underline{\hat{x}}_{n-1}\} \qquad (D.5)$$

where $\underline{y}_n$ is the current set of observations or measurements.

The error covariance can be updated to account for the current observation by the equation

$$P_n(+) = (I-GK_nC)\ P_n(-) \qquad (D.6)$$

The filter is implemented by choosing initial values $\underline{\hat{x}}_o$, $P_o(+)$, and GK_o, representing time t_o, and sequentially employing equations D.3 through D.6 every time the estimate is to be updated by Δt. In the case of the sensory mechanism model, $\underline{y}_n$ is the set of sensor signals at time t_n.

In the examples cited in section 6.1, it was assumed that the input spectrum and expected process noise intensity are constant over the maneuver segment being considered; so that A, Q, and Φ are constant. Observation noise intensity (R), however, was reset, at each sample, to be proportional to the square of the observation. This filter may also be implemented with time-varying system dynamics and noise intensities.

For the multi-sensory model application, Δt is not intended to represent a neural or biological sampling rate, but is only a convenient iteration interval for our simulation. We must be able to adjust this interval without affecting the performance (at least over frequencies that are lower than the sampling frequency). To accomplish this, at each iteration (n), diagonal elements of measurement and observation noise covariance matricies were chosen as follows:

$$\begin{aligned} Q_n &= Q\Delta t \\ R_n &= \rho y_n^2/\Delta t \end{aligned} \qquad (D.7)$$

where Q is the corresponding diagonal element of the power-spectral-density matrix, y_n is the corresponding observation (afferent signal) at time t_n, and ρ is a constant. Off-diagonal elements are zero.

The time-varying-gain filter responses shown in figures 6.1 and 6.2 were generated using the internal model of figure 6.3 with appropriate values of input bandwidth (β) and power-spectral density (Q). For the acceleration step,

$$Q = 2\beta\sigma_\alpha{}^2 \qquad (D.8)$$

with $\beta \simeq .001$ to approximate the spectrum of a step function in α. For the acceleration impulse, or step in angular velocity,

$$\sigma_\omega^2 = \frac{1}{\beta^2-\varepsilon^2}\left\{\frac{1}{2\varepsilon} - \frac{1}{2\beta}\right\}Q \qquad (D.9)$$

A wideband (impulse-like) spectrum for angular acceleration will be obtained when $\beta \simeq 1000$, $\varepsilon \simeq .001$. Therefore,

$$Q \simeq 2\ \varepsilon\ \beta^2\ \sigma_\omega^2 = 2000\ \sigma_\omega^2 \qquad (D.10)$$

The above development allows the a priori determination of the model parameters. For example, if subjects are experiencing acceleration steps of magnitude α^*, then $\sigma_\alpha^2 = (\alpha^*)^2$ would be the best value to use. Such accurate information about the stimulus and environment may be somewhat unrealistic unless the subject is well practiced and/or has active control of the stimulus.

The initial covariance of the Kalman filter, $P_o(+)$, was assumed to be zero; and the noise/signal "ratio" (ρ) was set to .001. Variations in ρ and $P_o(+)$ had little effect on the time-varying-filter results shown in figures 6.1 and 6.2.

☆U.S. GOVERNMENT PRINTING OFFICE: 1979- 671-056/111